MASTER

Proposal for a clamping force and ratio actuation system for a V-belt type CVT using rollers and a cable

Drabbels, R.G.J.

Award date:
2006

Proposal for a Clamping Force and Ratio Actuation System for a V-Belt Type CVT using Rollers and a Cable

R.G.J. Drabbels
Report number: DCT-2005-151

Supervisor:
Prof. Dr. Ir. M. Steinbuch

Coaches:
Ir. B. Bonsen
Ir. K.G.O. van de Meerakker

Master Thesis Committee:
Ir. B. Bonsen
Ir. K.G.O. van de Meerakker
Prof. Dr. Ir. M. Steinbuch
Dr. P.A. Veenhuizen
Dr. Ir. W.J. Witteman

Eindhoven University of Technology
Department of Mechanical Engineering
Section Control Systems Technology

Eindhoven, December 20, 2005

SUMMARY

To improve fuel economy, performance and driveability in modern day cars, continuously variable transmissions, or CVTs, are examined. Most belt type CVTs on the market are actuated by a hydraulic system. However, hydraulic actuation suffers from large pump losses that are the main cause for the low efficiency of most CVTs compared to manual transmissions. To get rid of the large hydraulic power loss and hence improve CVT efficiency, several electromechanical actuation concepts are examined. Subsequently, a new actuation concept is proposed with a transmission ratio on the pulley shaft, created using a roller system and a cable. In the new actuation system the actuation force is reduced, which reduces the power loss in the thrust bearing that transfers the actuation force to the pulley shaft. The new actuation design is modelled and efficiency measurements are performed. Furthermore several proposals for the complete transmission layout and cable actuation are presented.

This report contains a paper written for the *ASME Journal of Mechanical Design* and several appendices which give additional insight into the design process.

CONTENTS

Proposal for a Clamping Force and Ratio Actuation System for a V-Belt Type CVT using Rollers and a Cable

R.G.J. Drabbels, K.G.O. van de Meerakker, B. Bonsen
Technische Universiteit Eindhoven, Department of Mechanical Engineering,
P.O. Box 513, 5600 MB Eindhoven, The Netherlands

ABSTRACT

To improve fuel economy, performance and driveability in modern day cars, continuously variable transmissions, or CVTs, are examined. Most belt type CVTs on the market are actuated by a hydraulic system. However, hydraulic actuation suffers from large pump losses that are the main cause for the low efficiency of most CVTs compared to manual transmissions. To get rid of the large hydraulic power loss and hence improve CVT efficiency, several electromechanical actuation concepts are examined. Subsequently, a new actuation concept is proposed with a transmission ratio on the pulley shaft, created using a roller system and a cable. In the new actuation system the actuation force is reduced, which reduces the power loss in the thrust bearing that transfers the actuation force to the pulley shaft. The new actuation design is modelled and efficiency measurements are performed. Furthermore several proposals for the complete transmission layout and cable actuation are presented.

1. INTRODUCTION

In a car, a transmission is used to match the limited engine characteristics to the vehicle load. Traditionally, manual or stepped automatic transmissions only offer a limited number of transmission ratios, not allowing the engine to run in its full operating range. This decreases the efficiency of the engine. To improve fuel economy, performance and driveability, continuously variable transmissions, or CVTs, are examined. A CVT enables operation in a wider range of transmission ratios and the engine speed can be chosen independently of the vehicle speed. This way the engine can be operated more efficiently. It also gives a smoother ride because a CVT does not interrupt the torque transmission while changing ratio. Several different CVT principles are examined nowadays. The most important are toroidal and belt- or chain type CVTs. This article will focus on the actuation system of belt type CVTs. After a short description of the belt type CVT principle, different clamping force actuation systems are discussed. With the aim of improving the CVT efficiency, a new actuation system design is proposed. The new system is modelled and several strength tests and efficiency experiments are described and their results are presented. Furthermore some proposals for the complete transmission layout are given.

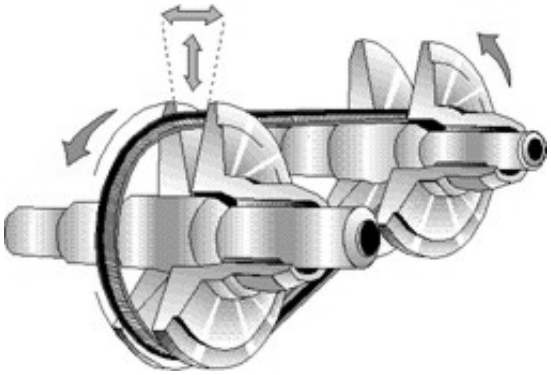

Fig. 1. Belt type CVT.

2. BELT TYPE CVT PRINCIPLE

In a belt type CVT (Fig. 1), torque is transmitted between two parallel shafts by means of a segmented steel V-belt. The belt runs over two pulleys that each consist of a fixed pulley sheave and an axially moveable sheave. The assembly of belt and pulleys is called ‘variator’. By adjusting the distance between the fixed and the moveable sheave, the running radius of the belt can be changed. Coordinated adjustment of the sheave distance on both shafts changes the transmission ratio between the shafts. To enable torque transmission by means of friction, while preventing excessive belt slippage, the belt is clamped between the pulley sheaves.

3. CLAMPING FORCE ACTUATION

3.1. Conventional hydraulic actuation

In most belt type CVTs on the market, the clamping force is generated by a hydraulic system. An oil pump provides the oil flow and pressure for the cylinders, which are fixed to the moveable pulley sheaves. The pump is most often coupled to the engine crankshaft, either directly or with a fixed transmission ratio. The pump is dimensioned to provide the demanded oil flow for maximum shifting speed while the engine is running at idle speed, and therefore the pump speed is minimal. At higher engine speeds, this results in excessive oil flows, while the oil still has to be kept pressurized to provide the clamping forces. The

drainage of these oil flows from high to low pressure is a direct power loss that significantly decreases the drive train efficiency [1]. This is the main cause for the low efficiency of most CVTs compared to manual transmissions. Apart from the pump loss, hydraulic actuation also suffers from oil leakage, friction and low stiffness.

3.2. Electromechanical actuation

To get rid of the disadvantages of a hydraulic actuation system, several electromechanical actuation concepts are examined. The main problem that has to be dealt with when designing an actuation system for a CVT, is the fact that the pulley sheave that has to be actuated is on a rotating shaft. In the conventional hydraulic actuation system the oil flows via a sealed connection from the pump through the rotating hollow pulley shaft to the cylinder. In an electromechanical actuation system, an electric motor provides the mechanical power needed for the clamping force actuation. The motor can either be placed on the pulley shaft or on the transmission housing. However, a motor fixed on the rotating pulley shaft is not desirable because of the high temperature inside the transmission, problems with the electric power supply and the increase in size and inertia of the shaft. When the motor is placed on the transmission housing, a constantly rotating motor shaft is not wanted because this results in a significant continuous power loss. Several electromechanical actuation concepts that deal with this problem will be discussed.

3.2.1. Non-rotating spindle

An example of an electromechanically actuated CVT is the dry hybrid belt CVT [2]. This CVT is designed for low power applications, with a torque capacity up to 85 Nm. Because of the absence of oil lubrication, the friction coefficient between the belt and the pulleys is high. As a consequence, the clamping forces can be kept low. The moveable pulley sheave is actuated with use of a non-rotating spindle, as shown in Fig. 2a. The nut is actuated by an electric motor via a gear transmission. The rotation of the motor is converted into a translation of the nut. Two deep groove ball bearings transfer the clamping force from the moveable sheave via the nut to the spindle and then back to the shaft. The bearings are both always rotating under load and at shaft speed, which causes continuous power loss.

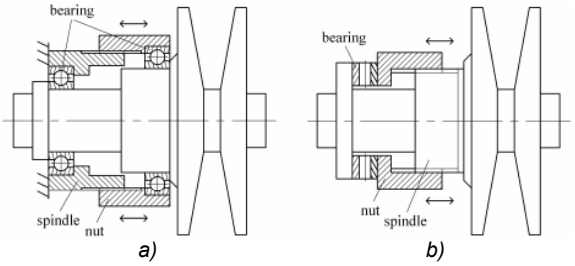

Fig. 2. a) Non-rotating spindle, nut and thrust bearings in dry hybrid CVT. b) Rotating spindle, nut and thrust bearing in EMPAct CVT.

In high power applications with a lubricated steel belt the axial bearing load is much higher. Larger thrust bearings are needed and the friction increases, which can lead to significant power loss.

3.2.2. Rotating spindle

One way of reducing the thrust bearing power loss, is to minimize the bearing rotation. An example is given by the electromechanical pulley actuation (EMPAct) system proposed by Van de Meerakker et al. [3]. The EMPAct system uses an electric motor to actuate a spindle nut via a double epicyclic gear set arrangement. The rotation of the motor is converted into a translation of the spindle. The spindle rotates at shaft speed, and the thrust bearing (see Fig. 2b), which is placed between the spindle nut and the pulley shaft, only rotates with adjustment velocity and only during ratio change. Because of its low speed, the power dissipation of the thrust bearing is very low, but the power loss of the two double epicyclic gear sets reduces this efficiency gain. A similar system is proposed by [4], and [5] shows a design where no thrust bearings are needed. Latter design uses a central screw shaft with opposite screw thread parts for each pulley sheave. Both sheaves of the pulley, which are each connected to one of the nuts engaging the screw thread parts, are simultaneously moving axially with respect to each other. The clamping force is transferred from one sheave via the screw shaft to the other sheave. Therefore no axial force has to be supported by the transmission housing. To actuate the screw shaft, again a double planetary gear set is needed.

3.2.3. Transmission ratio on shaft

Another approach for designing an electromechanical clamping force actuation system is putting a transmission ratio on the pulley shaft, between the moveable pulley sheave and a thrust bearing that enables actuation from the fixed transmission housing. The thrust bearing rotates at shaft speed, but only under a part of the clamping force load equal to the actuation force. Figure 3 shows the benefit of this approach. When the full clamping force is supported by thrust bearings (bearing load equals clamping force) at shaft speed, the power loss of the bearings plus an estimated pump loss of 150 W for remaining hydraulic functions like lubrication and cooling, is significant. When roller thrust bearings are used, the bearing losses are even higher than the total pump driving power of a conventional hydraulically actuated CVT [6] at high torques. When thrust ball bearings with the same load capacity are used, the bearing losses are smaller, but the bearing dimensions are much larger.
Reducing the actuation force gives a substantial decrease of the bearing power loss, since smaller thrust bearings can be used. Because of the reduced bearing load, the friction force inside the bearing is smaller, and the smaller bearing diameter also reduces the frictional torque.

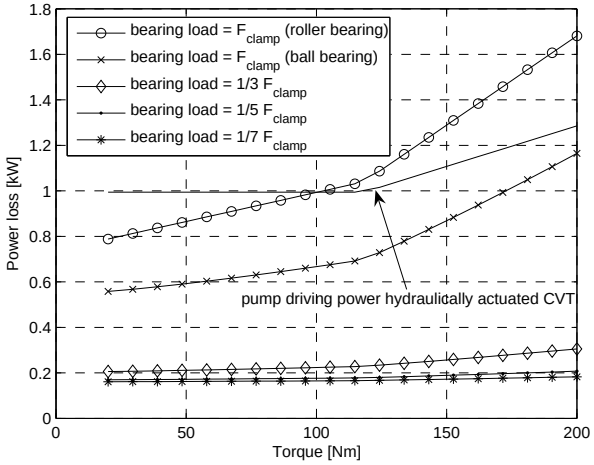

Fig. 3. Power loss in overdrive ratio at 1500 rpm.

The bearing losses are estimated with use of the equations formulated by bearing manufacturers [7]. For $\nu \cdot n \geq 2000$, the frictional torque M_R [Nmm] and frictional power N_R [W] are calculated with:

$$\begin{aligned} M_R &= M_0 + M_1 \\ &= f_0 \cdot (\nu \cdot n)^{2/3} \cdot d_M^3 \cdot 10^{-7} + f_1 \cdot P \cdot d_M \end{aligned} \quad (1)$$

And:

$$N_R = M_R \frac{n}{9550} \quad (2)$$

Where ν [mm^2/s] is the kinematical viscosity of the lubricant, n [rpm] is the rotational speed, M_0 [Nmm] is the frictional torque dependent on the speed, M_1 [Nmm] is the frictional torque dependent on the load, f_0 [-] is the bearing factor for frictional torque dependent on the speed, f_1 [-] is the bearing factor for frictional torque dependent on the load, P [N] is the bearing load and d_M [mm] is the mean bearing diameter $(d+D)/2$, with d the inner and D the outer diameter of the bearing.

Table 1.
Properties of the chosen thrust bearings for each transmission ratio between the pulley sheave and the thrust bearing.

TRANS-MISSION RATIO	THRUST BEARING TYPE	C [N]	d_M [mm]	f_0	f_1	L [10^6 revs]
1	cylindrical roller	105000	59	2.7	0.0015	6.5
1	ball	118000	112.5	1	$0.0012\left(\frac{F_a}{C_0}\right)^{0.33}$	7.6
1/3	ball	35500	48.5	1	$0.0012\left(\frac{F_a}{C_0}\right)^{0.33}$	5.6
1/5	ball	22400	30	1	$0.0012\left(\frac{F_a}{C_0}\right)^{0.33}$	6.5
1/7	ball	16600	23.5	1	$0.0012\left(\frac{F_a}{C_0}\right)^{0.33}$	7.2

The properties of the thrust bearings, chosen for each transmission ratio between pulley sheave and thrust bearing of Fig. 3, are presented in Table 1. In the table, C [N] is the basic dynamic load rating, C_0 [N] is the basic static load rating, F_a [N] is the axial bearing load and L is the basic rating life in millions of revolutions defined by:

$$L = \left(\frac{C}{P}\right)^p \quad (3)$$

Where p [-] is the life exponent, which equals 10/3 for cylindrical roller bearings and 3 for ball bearings.

When designing a transmission between the moveable pulley sheave and the thrust bearing, several basic transmission principles can be considered, such as a lever transmission or a gear transmission. However, because of the large maximum clamping force in high power CVTs, in a lever transmission the forces in the fulcrum of the lever(s) will be very large. Large contact and pivot forces are also a problem in gear transmission design. The fact that the transmission system is preferred to be very small enlarges these problems. A hydraulic transmission, consisting of cylinders with different piston areas, is also an option. Disadvantages of a hydraulic transmission are low stiffness, oil leakage and friction.

4. ROLLER CONCEPT CVT ACTUATION

4.1. The roller concept

To reduce the thrust bearing load, a transmission based on the roller concept is proposed. The basic principle of the roller system with cable is shown in Fig. 4a. A system with n_r rollers can establish a force

$$f = F \cdot (n_r + 1) \quad (4)$$

while applying an actuation force F. However, point a travels (n_r+1) times the distance of pointb .

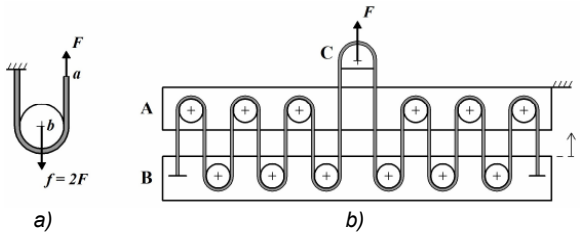

Fig. 4. a) Basic roller principle. b) Schematic view roller system.

A schematic representation of the roller system that is proposed is shown in Fig. 4b. It consists of two coupled identical roller systems. To establish a force between bodies A and B, only $1/(n_r/2+1)$ of this force needs to be applied to body C. Body C however travels $(n_r/2+1)$ times the distance of B. The tensile force in the cable equals half the actuation force applied to

body C. Using this system, a large force can be established between two bodies, while applying only a small actuation force dependent on the number of rollers. To use this roller system to apply the clamping force in a CVT, body A has to be connected to the pulley shaft and body B to the moveable pulley sheave. To allow rotation of the complete roller system, the actuation force *F* can be applied to body C via a thrust bearing.

4.2. Roller system specifications

The cable that is chosen is a synthetic rope. Synthetic ropes have a very small allowable curvature ratio compared to steel wire ropes with equal break strength. This results in a compact pulley system. The curvature ratio equals R_t/r, where R_t is the tread radius and *r* is the radius of the rope, as depicted in Fig. 5.

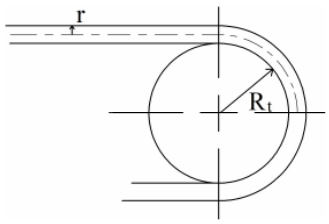

Fig. 5. The curvature ratio R_t/r.

Table 2 compares the, in terms of strength, fatigue life, flexibility and heat resistance, most suitable steel wire rope and synthetic rope. The synthetic rope is made of Technora fibre [8], which can be used at temperatures up to 200 °C for long periods of time without a significant decrease in strength. It has excellent fatigue resistance compared to other high tenacity fibres and negligible creep.

Table 2.
Steel wire rope compared to synthetic rope.

	MATERIAL	DIAMETER [mm]	MIN. BREAK STRENGTH [N]	R_t/r
Aircraft cable (7x19)	galvanized carbon steel	3	8900	24
Tech 12	Technora	3	11210	8

The smallest manufactured Tech 12 rope has a diameter of 3 millimetres. This comes down to a minimum allowable roller tread diameter of 24 millimetres. With the demand that the system must be able to generate a clamping force of 50 kN (maximum primary torque of about 300 Nm), and a safety factor for the rope strength of about three, this results in a total transmission ratio of seven (output force / input force). The maximum rope force at a clamping force of 50 kN equals about 3600 N, and the maximum force on the rollers is 7200 N. The resulting total roller system consists of twelve rollers. A larger number of rollers will result in a larger transmission ratio and a larger safety factor, but the system will increase in size and the additional decrease of the thrust bearing power loss is minimal. The thrust bearing needed at a transmission ratio of seven has an outer diameter of only 32 millimetres, which is an advantage for the actuation system design because it fits inside the pulley shaft.

5. ACTUATION SYSTEM DESCRIPTION

5.1. Roller system

The roller system consists of two rings, each containing six small rollers. One of the rings is fixed on the shaft, the other ring can slide along the shaft and is connected to the moveable pulley sheave. The moveable pulley sheave is fitted on the shaft with a spline to prevent rotation compared to the fixed pulley sheave. The roller configuration within the rings is shown in Fig. 6. The rope is winded through the rollers. On the slider ring, two rollers are turned in a way that their centrelines are orientated tangential to the shaft. They are used to guide the rope from outside to inside the hollow pulley shaft. The rollers are made of rolling bearings with an outer ring that contains a groove for the rope.

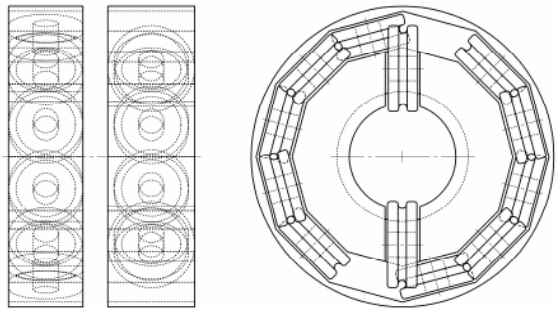

Fig. 6. Roller configuration.

5.2. Shaft layout

The total shaft layout is shown in Fig. 7. The two rings that contain the rollers correspond as indicated with body A and B of Fig. 4b.

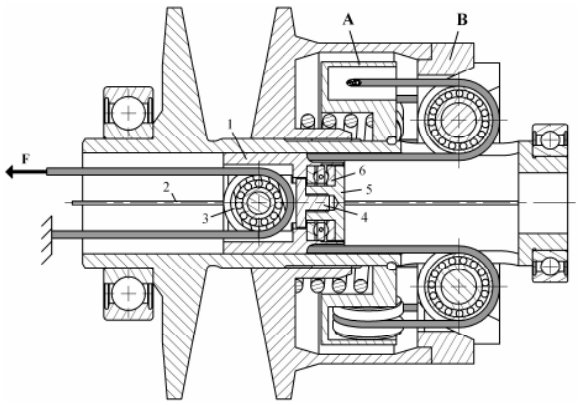

Fig. 7. Shaft layout with cables.

The mechanism that enables actuation of the roller system from the fixed trans-mission housing is placed inside the hollow pulley shaft. A small tube (1) fulfils

the task of body C in Fig. 4b. It can slide inside the pulley shaft along a thin rod (2) that prevents rotation compared to the shaft, so that the ropes do not wind up. The distance that is covered by the tube during shifting from low to overdrive ratio fits inside the shaft. A roller (3) is placed inside the tube and connected with the tube via part 4, part 5 and a thrust ball bearing (6), so that the roller does not rotate compared to the transmission housing. This roller system further reduces the actuation force by a factor of two. The thrust bearing transfers the actuation force to the roller system. The axial reaction force on the pulley shaft, which equals *2F*, is supported by the deep groove ball bearing left of the fixed pulley sheave.

Between the fixed ring (A) and the moveable pulley sheave a preloaded spring can be placed. The spring provides a force in the direction of the belt clamping force, dependent of the spring stiffness and the compression of the spring. Therefore, the spring force varies with the variator ratio. The spring force decreases the needed actuation force and the rope force. Furthermore, the spring makes sure that there always is a force that keeps the belt clamped, even when the actuation force fails.

6. MODELLING

To obtain an estimation of the losses in the roller system, the power losses in the system are modelled. The losses in the rollers, which are made of rolling bearings, can be modelled with the bearing equations Eq. (1) and Eq. (2) as defined before, with the only difference that for $\nu \cdot n < 2000$ M_0 is calculated slightly different, see Eq. (5). With use of the equations the frictional torque and frictional power loss of the rollers can be estimated.

$$\begin{aligned} M_R &= M_0 + M_1 \\ &= f_0 \cdot 160 \cdot d_M^3 \cdot 10^{-7} + f_1 \cdot P \cdot d_M \end{aligned} \tag{5}$$

Modelling of the rope is more complicated. To obtain an estimation of the losses in the rope, a simplified model of the rope is considered, like shown in Fig. 8.

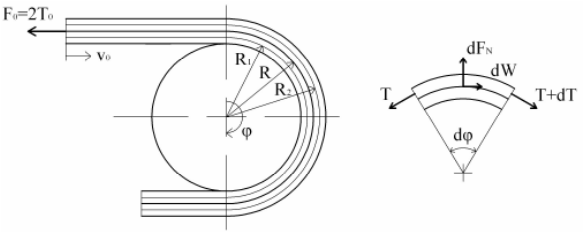

Fig. 8. 2-layer rope model.

The rope is assumed to consist of two layers, which slip along each other because of their different running radius over a roller. Although in reality the strands of the rope slide over each other in various directions, it is assumed this model gives a reasonable estimation of the friction losses inside the rope. The relative speed between the two layers equals:

$$v_{rel} = \left(\frac{R_2}{R} - \frac{R_1}{R} \right) \cdot v_0 \tag{6}$$

Where v_0 [m/s] is the initial rope speed. The right picture in Fig. 8 shows the forces acting on an element of the upper rope layer, which is assumed to slip over the lower layer with the relative speed. Summing the forces in vertical (radial) direction gives:

$$dF_N = T \cdot d\varphi \tag{7}$$

Summing the forces in horizontal (tangential) direction gives:

$$-\mu \cdot dF_N = dT \tag{8}$$

With μ [-] the coefficient of friction between the layers. Substituting Eq. (7) in Eq. (8) and integrating the resulting equation gives:

$$-\mu \cdot \int_0^{\varphi} d\varphi = \int_{T_0}^{T_1} \frac{1}{T}\, dT$$

$$\frac{T_1}{T_0} = e^{-\mu\varphi}$$

The tensile force $T(\varphi)$ [N] in the upper layer can be calculated with:

$$T(\varphi) = T_0 \cdot e^{-\mu\varphi} \tag{9}$$

Where T_0 is the initial tensile force in the upper layer of the straight part. The frictional power loss inside the rope and the efficiency of the rope η_r [-] when moving over one roller can now be estimated with:

$$P_{loss} = \left(T_0 - T(\varphi)\right) \cdot v_{rel} \tag{10}$$

$$\begin{aligned} \eta_r &= \frac{P_0 - P_{loss}}{P_0} \\ &= \frac{2T_0 \cdot v_0 - P_{loss}}{2T_0 \cdot v_0} \end{aligned} \tag{11}$$

Where P_0 [W] is the initial power in the rope. A computer model has been created which takes into account the roller bearing losses, the friction losses caused by the slip inside the rope and a coulomb friction of the sliding contact of ring B of Fig.7. The roller system efficiency predicted by the model is depicted in Fig 9.

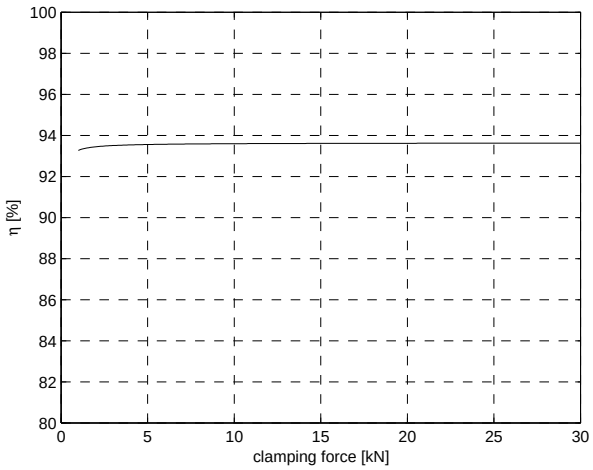

Fig. 9. Model predicted roller system efficiency.

7. EXPERIMENTS

To validate the rope specifications for this application, the rope is tested with a pulling bench. Furthermore a test rig is built to test the roller system and to measure its efficiency.

7.1. Rope break strength

Like shown in Fig. 4b, both ends of the rope have to be fixed to the moveable ring of the roller system. For this purpose the rope is winded several times around a pin to transmit a large part of the ropes tension to the pin by friction, and then tied up around a second pin with a buntline hitch [9,10]. The conventional way of fixing a rope, using an eye splice, is not used in this case because it takes too much space. To test the rope and the way it is fixed, the break strength of several samples is measured with a pulling bench. The rope is fixed at both ends in the same way as described above. The results of six break strength tests are presented in Table 3. Three tests are performed with dry rope and the other tests are performed with ropes that were drenched in automatic transmission fluid (ATF) for two months to test the resistance of Technora to ATF oil. It is important that the ATF does not have a negative influence on the properties of the rope because this oil is normally present in belt type CVTs. The test results show even a positive influence on the average break strength, which can be caused by the lubrication properties of the ATF. Because of the small number of test however no definite conclusions can be drawn.

Table 3.
Rope break strength test results.

TEST	BREAK STRENGTH [N]	
	DRY	AFTER 2 MONTHS IN ATF
1	7441	7339
2	7283	7506
3	7446	7746
AVERAGE	**7390**	**7530**

The test results further show that the way the rope is fixed significantly decreases the break strength of the rope compared to the specifications provided by the manufacturer. All samples of the rope snapped at the point were they were winded around the first pin. Therefore further research on this topic might be useful.

7.2. Roller system test set-up

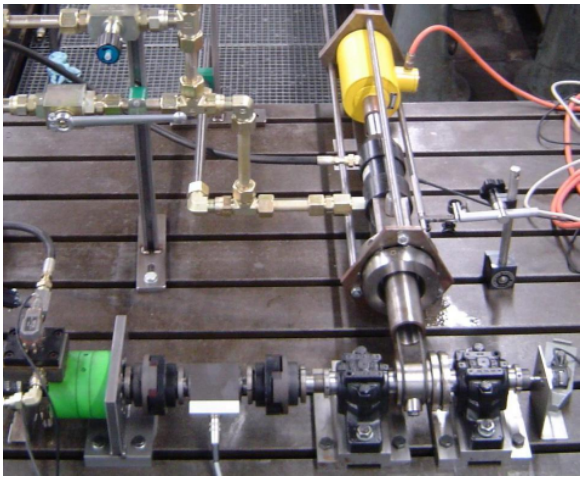

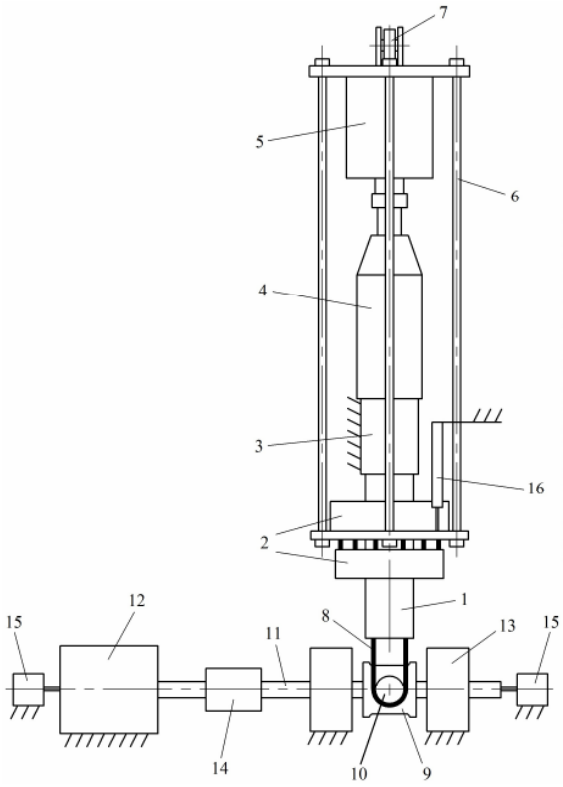

Fig. 10. The roller system test set-up.

In order to test the roller system a test set-up is designed, see Fig. 10. To simplify the test set-up, only one shaft (like shown in Fig. 7) is built, which does not rotate. The extra roller system inside the shaft with the thrust bearing and one roller is left out, just like the two pulley sheaves and the spring, so that only the shaft and the two rings remain. The shaft (1), together with the two rings (2) that contain the rollers, is mounted to a block (3) which is fixed to the test bed. To simulate

the pulley sheaves with the belt in between, a hydraulic cylinder (4) is used, which provides the counterforce for the roller system. The cylinder is connected with the moveable ring of the roller system via a load cell (5) and three pulling rods (6). A roller bearing (7) supports the weight of the load cell.
The roller system is actuated by winding the rope loop (8) around a drum (9) with use of a pin (10) on the drum that fulfils the task of body C in Fig. 4b. The shaft (11) of the actuation system is driven by a hydraulic motor (12), and fixed to the test bed via bearings units (13) on both sides of the drum. In between the drum and the hydraulic motor a torque sensor (14) is connected, and at both ends a rotary encoder (15) is connected to the shaft.

Table 4.
Test set-up sensor specifications

MEASURED VARIABLE	SENSOR	MANUFACTURER + TYPE	RESOLUTION
T_{act}	torque sensor	HBM T20WN/200Nm	0.4 Nm
ω_{drum}	rotary encoder	Heidenhain ROD 1020	$4.4*10^{-4}$ rad
F_{clamp}	load cell	HBM C3	100 N (after calibration)
v_{ring}	digital length gauge	Heidenhain SPECTO ST 3078	1 m

With the roller system set-up, efficiency measurements are performed. The actuation torque T_{act} [Nm] and the angular speed of the drum ω_{drum} [rad/s] are measured to calculate the input power, and the output force F_{clamp} [N] and the speed of the moveable ring v_{ring} [m/s] are measured to calculate the output power. Table 4 shows some specifications of the sensors that are used in the test set-up.

7.3. Efficiency measurements results

Figure 11 shows the relation between the actuation force, calculated from the actuation torque and the radius on which the rope loop is winded around the drum, and the actual clamping force.

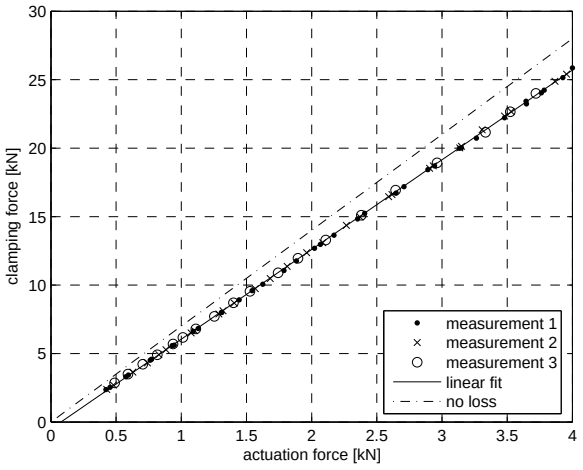

Fig. 11. Roller system friction loss.

Three independent measurements nearly show the same results. It appears that the relation between the actuation force and the clamping force can be approximated with a linear fit:

$$F_{clamp} = c \cdot F_{act} + F_{clamp,0} \tag{12}$$

This indicates that the losses in the system consist of a constant part with value $F_{clamp,0}/c$, and a part that is dependent on the clamping force. Because of the transmission ratio i [-] of seven, in theory, the clamping force equals seven times the actuation force (no loss).

$$F_{clamp,th} = i \cdot F_{act} \tag{13}$$

The system efficiency η [-] can be calculated with:

$$\eta = \frac{F_{clamp}}{F_{clamp,th}} \tag{14}$$

By substituting Eq. (12) and Eq. (13) in Eq. (14), the efficiency can be estimated.
Figure 12 shows this estimation derived from the linear fit, together with the roller system efficiency calculated from the measurement data by:

$$\eta = \frac{P_{out}}{P_{in}} = \frac{F_{clamp} \cdot v_{ring}}{T_{act} \cdot \omega_{drum}} \tag{15}$$

Where P_{in} [W] and P_{out} [W] are respectively the input power and the output power of the roller system. It appears that the linear relation of Eq. (12) gives a good estimate of the roller system efficiency. Only at clamping forces below 5 kN the difference with the measured efficiency becomes rather large.

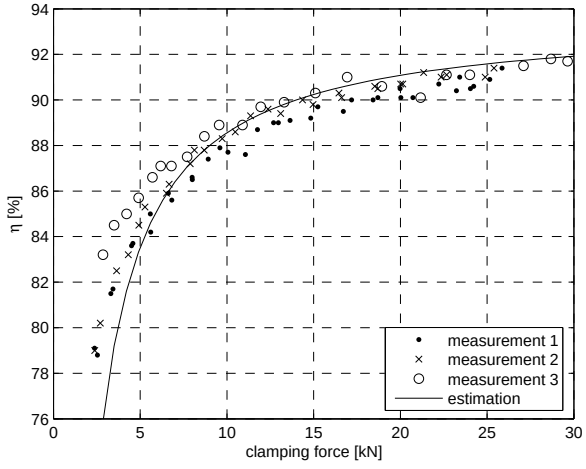

Fig. 12. Roller system efficiency.

Figure 13 shows the efficiency predicted by the model compared to the measurement results. It appears that the model results do not correspond to the measurement data very well. It seems that an additional friction loss is present in the roller system, which is not included in the model. This additional

friction loss is assumed to be mainly caused by the unexpected considerable friction force between the rope and the rollers.
The rope specifications state a rope diameter of 3 mm. The actual rope diameter appeared to be somewhat larger, especially at small rope loads. The grooves in the outer rings of the rollers however are designed assuming a rope diameter of 3 mm. Furthermore the grooves have rather steep sides, like shown in Fig. 14a. Because of the larger rope diameter and the shape of the grooves, the rope gets clamped inside the groove. Especially when entering and leaving the roller, this can cause significant friction between the rope and the roller groove sides. Adding a constant friction force at each roller improves the model results significantly. The efficiency predicted by the adjusted model with an additional friction force of 13 N at each roller is also plotted in Fig. 13.

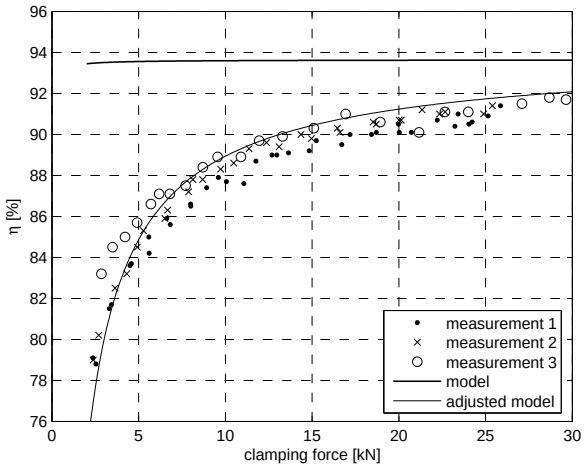

Fig. 13. Efficiency predicted by the original model and the adjusted model compared with the measurement results.

It is proposed to adjust the grooves to a shape shown in Fig. 14b, which can significantly improve the roller system efficiency and increase the lifespan of the rope.

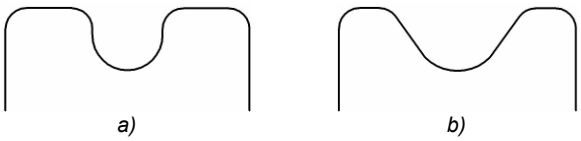

Fig. 14. a) Initial roller groove shape. b) Proposed adjusted roller groove shape.

8. ROLLER CVT LAYOUT PROPOSAL

The CVT consists of two pulley shafts, each with its own roller system to move the moveable pulley sheave and apply the clamping force. There are several possibilities to connect the engine and the differential with the input and output shaft of the CVT variator. Two possible layouts will be discussed here, together with proposals for the rope actuation.

8.1. CVT layout

The two rope ends coming out of the shaft constitute a limitation in the way the transmission is connected to the engine and the differential. The rope ends leave the shaft at the opposite side of the moveable pulley sheave. To keep the belt in line, the moveable pulley sheave on the primary shaft of the variator should be placed on the opposite side compared to the moveable pulley sheave on the secondary shaft.

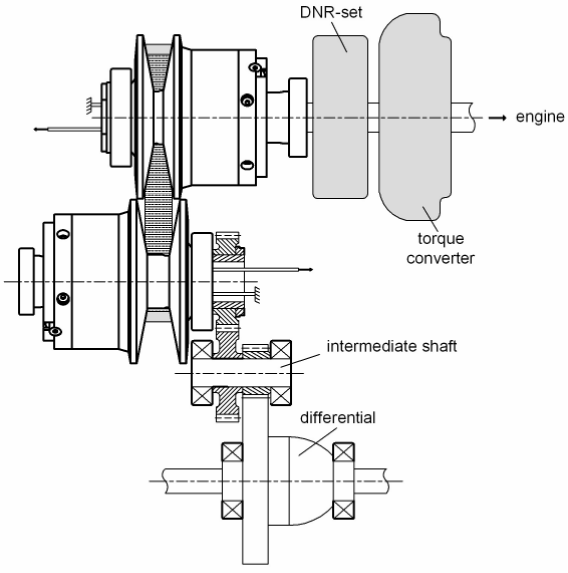

Fig. 15. Transmission layout with intermediate shaft.

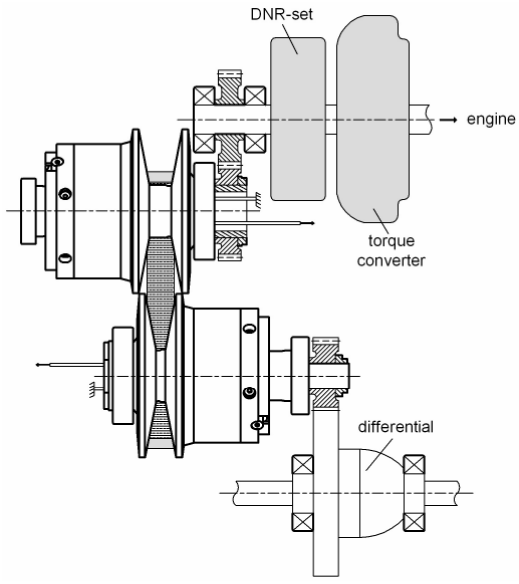

Fig. 16. Transmission layout with parallel shaft.

Figure 15 and Fig. 16 show two possible layouts. In Fig. 15, the engine is directly connected to the primary variator shaft via the torque converter and the DNR set. The moveable pulley sheave on the primary shaft is located at the engine side, so that the ropes come

out at the free end of the shaft. Between the secondary variator shaft and the differential, an intermediate shaft is placed to change the rotation direction. It also functions as a final reduction gear. Figure 16 shows an alternative layout, where the moveable pulley sheave of the primary variator shaft is placed on the opposite side. To create space for the ropes to come out of the pulley shaft a parallel shaft, connected to the primary shaft with a fixed gear, is used to connect the engine with the transmission. In this case the intermediate shaft at the secondary side can be left out. To make the transmission more compact, the parallel shaft can be placed between the two variator shafts.

8.2. Rope actuation

To apply a clamping force, the free rope end that comes out of each variator shaft has to be actuated. Shifting of the variator is achieved by creating a difference in clamping force between both pulleys, allowing displacement of the moveable sheaves. When the rope at one shaft is pulled, the clamping force increases and the belt is pushed outwards. The tension in the belt causes the belt to be pulled inwards at the other pulley. When the difference in clamping force between the pulleys is large enough, the pulley sheaves start to move and the variator ratio changes.
While shifting, at one variator shaft the moveable pulley sheave moves in the opposite direction of the clamping force acting on the sheave. Energy must be supplied for the sheave displacement. At the other shaft, the moveable pulley sheave moves in the same direction as the clamping force acting on the sheave and energy is released. For the roller system this means that at one shaft the rope has to be pulled out of the shaft, and at the other shaft the rope is pulled into the shaft. By coupling both roller systems, energy can be exchanged between the two moveable pulley sheaves. This reduces the power needed for changing the variator ratio. Only the energy to overcome the losses during ratio change has to be supplied.

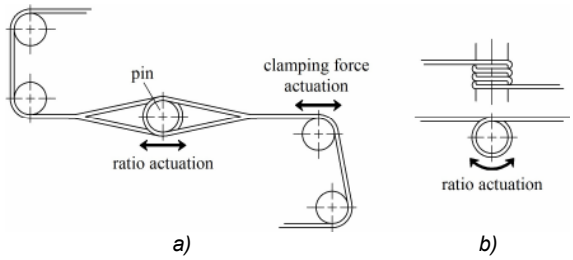

Fig. 17. a) Possible rope actuation. b) Alternative ratio actuation.

Figure 17a shows a possible rope actuation concept. An eye splice is created at both rope ends and wrapped around a pin, which is actuated with use of an electric motor. By translating the pin like indicated in the figure, the variator ratio can be changed. Tightening the rope by translating one of the rollers that guide the rope from the primary pulley shaft to the secondary shaft with another electric motor changes the clamping force. Fig. 17b shows an alternative for the ratio actuation where one rope end is winded around a drum and at the same time the other rope end is unwound. When the rope ends are connected, slip between the rope and the drum must be prevented. A difference in clamping force between the primary and secondary pulley can be generated by coordinated control of the rope forces with use of both electric motors.

CONCLUSION

The pump loss in a conventional hydraulically actuated CVT is the main cause for the relatively low efficiency of a CVT compared to a manual transmission. Electromechanically actuated CVTs are examined to improve CVT efficiency and a new actuation system design is proposed. On the pulley shaft, a transmission ratio is created using a roller system and a cable. This way the load on the thrust bearing that transfers the actuation force from the transmission housing to the rotating pulley shaft is reduced, which reduces the bearing power loss. In theory, the new system design shows great potential for an actuation system with an improved efficiency compared to a hydraulically actuated CVT. Efficiency measurements on a test set-up show that the efficiency of the roller system on the pulley shaft is somewhere between 84 – 94 percent in normal working conditions. After comparison with the efficiency predicted by the roller system model, it is expected this efficiency can be improved by adjusting the shape of the grooves in the rollers. Tests show that the break strength of the chosen Technora rope for the roller system is significantly decreased by the proposed way of fixing the rope. Therefore further research on this topic might be useful. Several layouts for a CVT with the new actuation system are proposed. In future research, the complete CVT with roller systems should be further designed, and a prototype should be developed to measure the complete CVT efficiency.

REFERENCES

[1] Ide, T., 2000, “Effect of Belt Loss and Oil Pump Loss on the Fuel Economy of a Vehicle with a Metal V-Belt CVT”, FISITA World Automotive Congress, Seoul

[2] Tsukasa Yuki, Mitsunao Takayama, Hisato Kato, 1995, “Development of dry hybrid belt CVT”, JSAE Review 16, pp. 251-256

[3] Meerakker, K.G.O. van de, Rosielle, P.C.J.N., Bonsen, B., Klaassen, T.W.G.L., 2004, “Design of an Electromechanical Ratio and Clamping Force Actuator for a Metal V-belt Type CVT”, Eindhoven, The Netherlands

[4] Kapaan, H.J., et al., 2000, “Pulley Set for a Continuously Variable Transmission Unit”, PCT Pub. No. WO 00/60256, SKF Engineering & Research Centre B.V., Nieuwegein, The Netherlands

[5] Kapaan, H.J., et al., 2003, “Continuously Variable Transmission with Axially Movable Pulley Hub Units”, PCT Pub. No. WO 03/036134

[6] Albers, P.H.W.M., Veenhuizen, P.A., 2005, “Fuel Economy Benefits of Advanced Techniques for CVT Actuation and Control”, 10th EAEC European Automotive Congress, Belgrade

[7] Link from FAG website (http://www.fag.com), http://medias.ina.de/medias/en!hp.tg.cat/tg_rot*CHEBHCFE;aIitlvjH_fB_, 20-12-2005

[8] TEIJIN website, http://www.teijin-aramid.com/eng/Index.htm, 20-12-2005

[9] http://www.realknots.com/knots/hitches.htm #buntline, 20-12-2005

[10] Ashley, C.W., 1985, “The Ashley Book of Knots”, Faber and Faber, London

APPENDIX A: ACTUATION SYSTEM DESIGN

In this appendix some aspects of the actuation system design are further explained.

A1. Roller configuration

The number of rollers determines the transmission ratio of the roller system. More rollers result in a larger transmission ratio. The roller system is preferred to be of approximately the same size as the hydraulic cylinders of a conventional CVT. Different roller configurations are examined to determine the best configuration taking account of the number and size of the rollers, the size of the total roller system, the construction simplicity and corresponding manufacturing costs. For the design of the roller system around the pulley shaft, two basic roller configurations are proposed. For an optimal use of the available space, while accommodating the maximum number and size of the rollers, the rollers should be placed according to Fig. A.1. However, placing the roller axles becomes a problem when the number of rollers increases. Also the manufacturing of the ring and the assembling of the axles and rollers can become rather complicated.

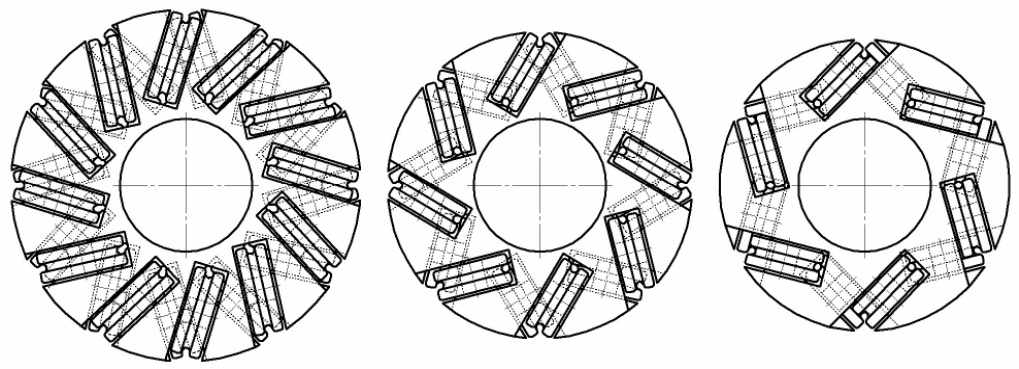

Fig. A.1. Rollers in "star" configuration.

Another possible roller configuration is shown in Fig. A.2. The manufacturing of the ring and the placing and assembling of the axles and rollers are less complicated, but the size increases significantly with an increasing number or size of the rollers. A solution could be a second ring of rollers inside the first ring. This however again increases the complexity of the construction.

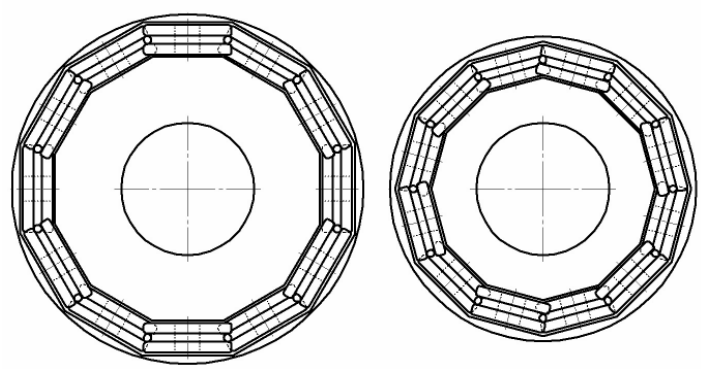

Fig. A.2. Roller axles oriented radial to shaft.

After analyzing the forces in the roller system, together with the rope specifications, a roller system with a total number of twelve rollers with a tread diameter of 24 mm is chosen. At this rather small number of rollers, and this size of the rollers, the roller configuration of Fig. A.2 only results in a very small increase in size of the roller system compared to the configuration of Fig. A.1. Because the roller system construction of Fig. A.2 is less complicated, this configuration is chosen.

To be able to actuate the roller system from the fixed transmission housing, the rope is guided inside the pulley shaft. To realize this, at least one roller of one of the rings can be turned in a way that its centreline is orientated tangential to the shaft. To ensure that the forces on the pulley system are divided symmetrically compared to the pulley shaft, two rollers are turned to guide the rope inside the shaft like shown in Fig. A.3a. The system is now split into two identical roller systems, which can be coupled by linking the two rope ends inside the shaft. The other rope ends are connected to the ring with the turned rollers. Because the two roller systems are linked, they can be actuated symmetrically by pulling the rope loop inside the shaft. The actuation force is now a seventh of the clamping force. An alternative roller configuration is shown in Fig. A.3b, where the system is split into three identical roller systems. Linking these three systems is somewhat more difficult and furthermore the actuation force increases to more than a fifth (3/14) of the clamping force, because the transmission ratio between the clamping force and the actuation force decreases.

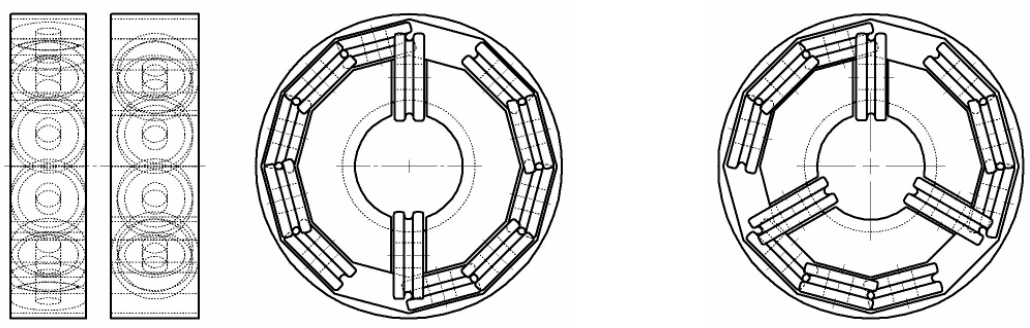

Fig. A.3. a) Chosen roller configuration. b) Alternative roller configuration.

For the sake of completeness some alternative “star” configurations with twelve rollers are shown in Fig. A.4. When a larger transmission ratio between the clamping force and the actuation force or a lower rope load is desired, and therefore more rollers are needed, this configuration can be very useful to keep the size of the roller system minimal.

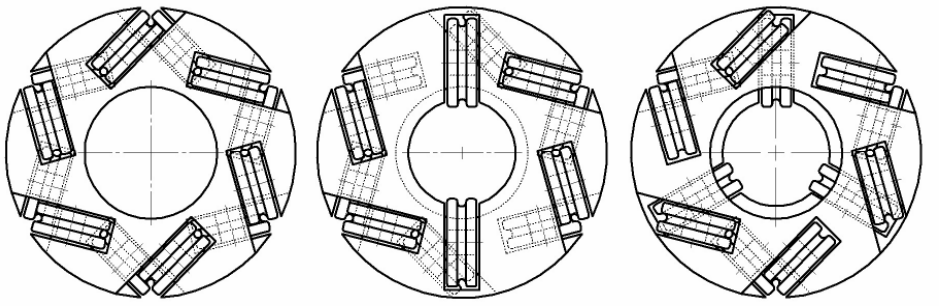

Fig. A.4. Alternative “star” configurations.

A2. Roller system design

The roller system presented in Fig. A.3a consists of two rings with rollers. When the shaft is rotating, the rollers are pushed outwards by the centrifugal force. The rollers are assembled between two Teflon rings to prevent large friction forces between the roller and its housing, like shown in Fig. A.5. Teflon is used because of the low coefficient of friction between Teflon and steel. The roller axle has fits on both sides of the roller and is screwed into the inner part of the ring. The two turned rollers are also enclosed by two Teflon rings, and their axles are assembled via slots.
Both ends of the rope of the roller system are fixed to the moveable ring. For this purpose the rope is winded several times around a pin to transmit a large part of the ropes tension to the pin by friction, and then tied up around a second pin with a buntline hitch. The conventional way of fixing a rope, using an eye splice, is not used in this case because it takes too much space.

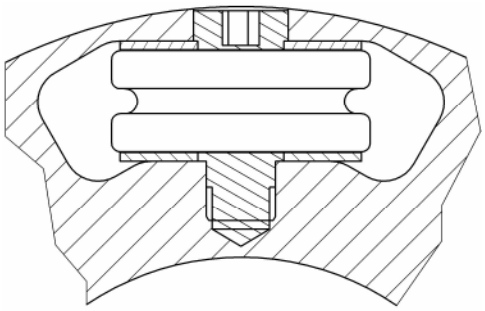

Fig. A.5. Roller fixed between Teflon rings.

A3. Shaft layout

The intended shaft layout design contains the two rings (A and B) with rollers around the pulley shaft, like shown in Fig. A.6. One ring (A) fixed to the shaft and the other (B) fitted on the shaft, free to move axially along the shaft towards and away from the fixed ring. Rotation of the rings compared to the pulley shaft must be prevented, and the moveable ring must be connected to the moveable pulley sheave. Furthermore the shaft layout must be designed in a way that the assembly of all parts is possible.

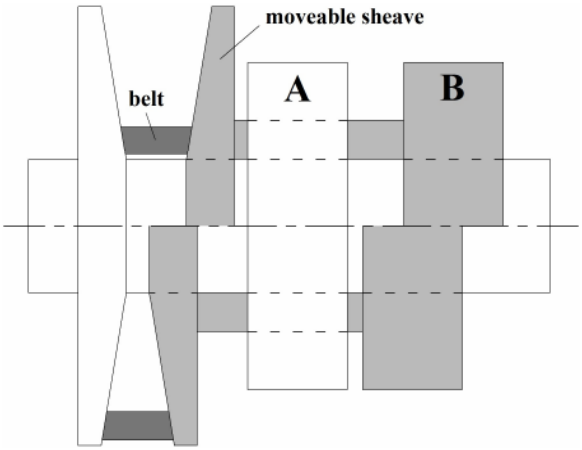

Fig. A.6. Schematic shaft layout design.

A possible way to fix ring A to the shaft is by placing two or more supports between the ring and the shaft like shown in Fig. A.7. Ring B can now be connected to the pulley sheave through the spaces between the shaft and the fixed ring A. The fixed pulley sheave is normally manufactured in one piece with the shaft, so the moveable pulley sheave cannot be assembled from the left side in Fig A.6. Therefore, the supports between the fixed ring and the shaft must be removable. The connection between the supports and the shaft is rather problematic, because the supports must be able to withstand up to 6/7 of the maximum clamping force.

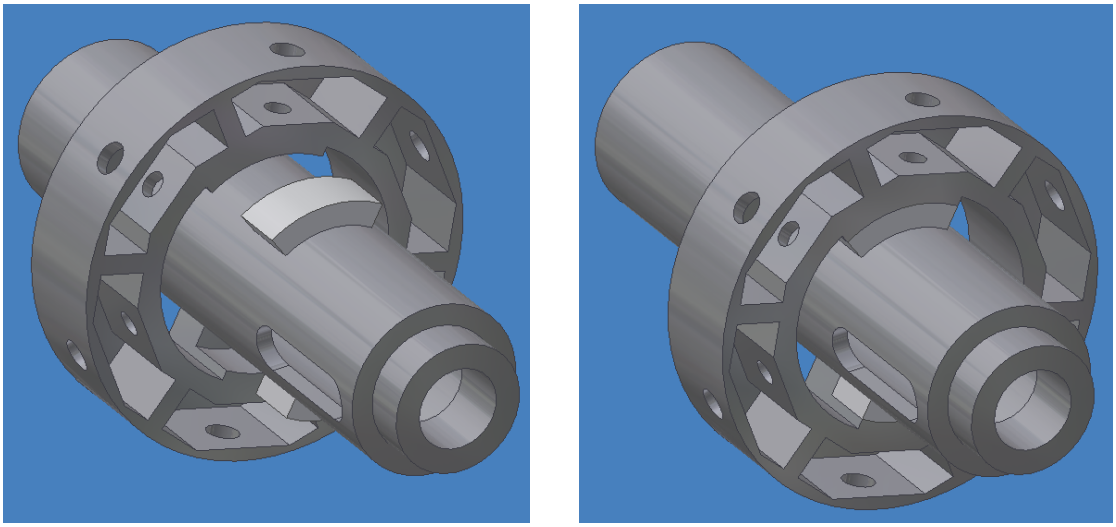

Fig. A.7. Ring fixed on pulley shaft with use of supports.

An alternative way to connect the moveable ring to the moveable pulley sheave is around the outside of ring A. This way is used in the final design that is shown in Fig. A.8 and Fig. A.9, because it has several advantages. Ring A can now be fixed to the shaft by a fix-ring placed in a groove in the shaft. When the moveable pulley sheave is assembled, the moveable ring is placed on the shaft, just passed the groove in the shaft. Now the two halves of the fix-ring can be placed into the groove and the ring is moved back over the fix-ring to lock it up. Because the forces on ring A always act in the direction of the moveable ring B, ring A will not move in the opposite direction which would unlock the two half fix-rings. If a preloaded spring is placed between the moveable pulley sheave and the fixed ring A, like proposed in the paper, the spring force will help the ring to retain its position. Rotation of ring A compared to the pulley shaft is prevented by a small key. The moveable pulley sheave and the moveable ring that is connected to it are fitted on the shaft with a spline, which prevents rotation compared to the shaft.
The rollers that guide the rope inside the pulley shaft are placed on the moveable ring. This increases the space inside the shaft for the movement of the construction that enables actuation of the roller system from the fixed transmission housing. Furthermore the transmission ratio of the roller system would only be 6:1 instead of 7:1 when the turned rollers are placed on the fixed ring.

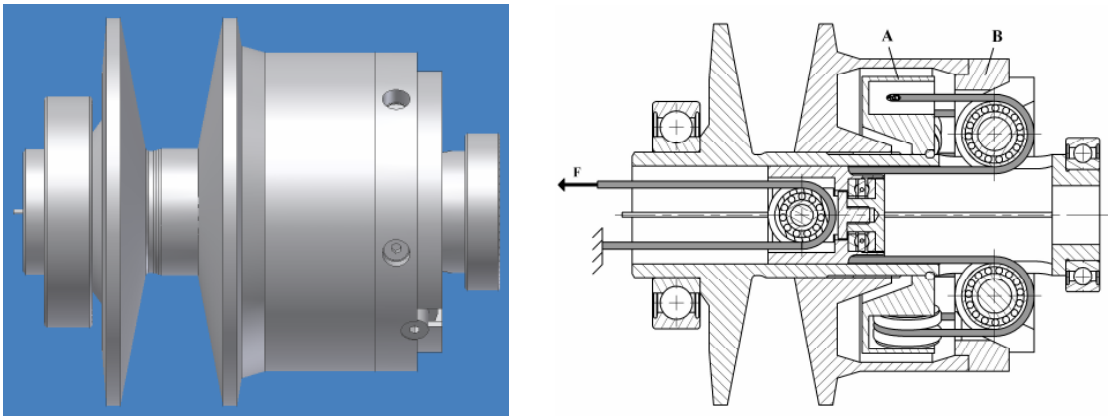

Fig. A.8. Final shaft layout design.

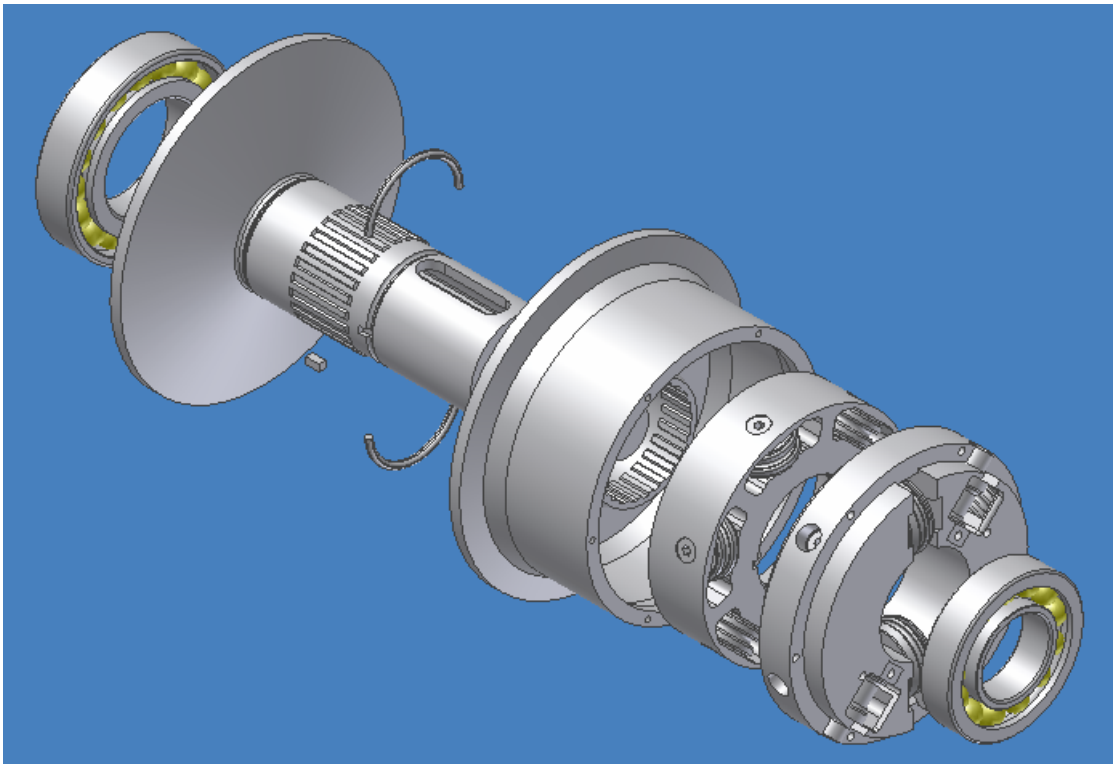

Fig. A.9. Exploded view of final shaft layout design.

The construction of Fig. A.10 is proposed to make it possible to actuate the roller system from the fixed transmission housing without the ropes winding up. The rope inside the shaft is guided from the first to the second part of the roller system shown in Fig. A.3a and rotation compared to the shaft is prevented. The roller system can now be actuated from the fixed transmission housing via a thrust bearing. With an extra roller the actuation force is further reduced by a factor of two. The use of a spindle or a hydraulic cylinder can also be considered to actuate the roller system inside the shaft.

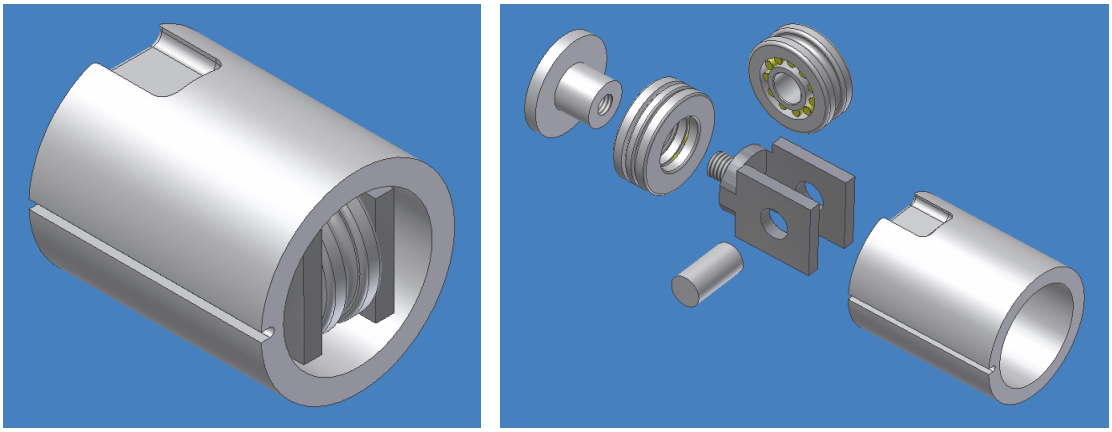

Fig. A.10. Thrust bearing and roller construction inside shaft.

APPENDIX B: FEM CALCULATIONS

B1. Pulley shaft

Due to the forces on the pulley sheaves, the pulley shaft is loaded with a torque and a shear force which causes a bending moment. An approximation for the shear force F_s can be given by:

$$F_s = \tan(\alpha) \cdot F_{clamp} \tag{B.1}$$

Where α [°] is the pulley wedge angle and F_{clamp} is the applied clamping force. With α = 11° and a maximum clamping force of 50 kN, this results in a maximum shear force of approximately 10 kN. The maximum torque T_{shaft} in the secondary shaft is assumed to be approximately 500 Nm. The shaft must withstand the stresses that result from these loads, without any plastic deformation. To be able to construct the shaft, the stresses have to be calculated. Because of the rather complex shaft geometry this cannot be done by hand. Therefore, the CAD drawings from Inventor are used in a finite element method (FEM) program. This makes it possible to easily compare different construction designs. For the pulley shaft the groove for fixing ring A and the slots for guiding the cables into the shaft are the most critical, because it is assumed that around them the largest stresses occur.

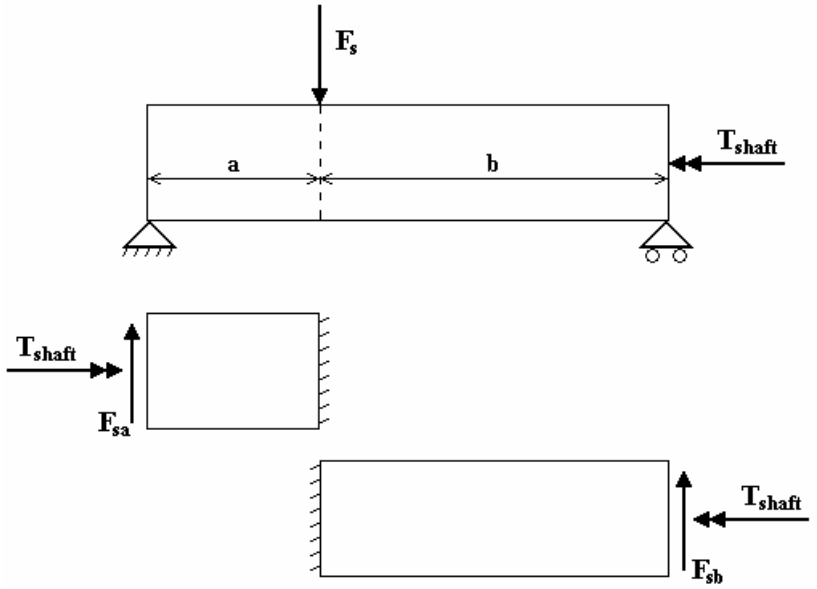

Fig. B.1. Schematic representation of the loads on the pulley shaft due to the forces on the pulley sheaves.

Figure B.1 gives a schematic representation of the loads on the pulley shaft. To be able to analyze the stresses in the shaft with the FEM computer program, the shaft is split into two parts between the pulley sheaves. The torque only acts on one of the parts, depending on the side of the shaft where the engine (primary shaft) or the differential (secondary shaft) is connected. The shear force on each part of the shaft can be calculated with:

$$F_{sa} = \left(\frac{b}{a+b} \right) \cdot F_s \tag{B.2}$$

$$F_{sb} = \left(\frac{a}{a+b} \right) \cdot F_s \tag{B.3}$$

Apart from the forces on the pulley sheaves, the roller system also introduces an internal force in the shaft between the fixed ring and the pulley sheave fixed on the shaft as indicated in Fig. B.2. One side of the groove in the shaft is loaded with the force acting on the fixed ring of the roller system, which has a maximum value of 6/7 of the maximum clamping force.

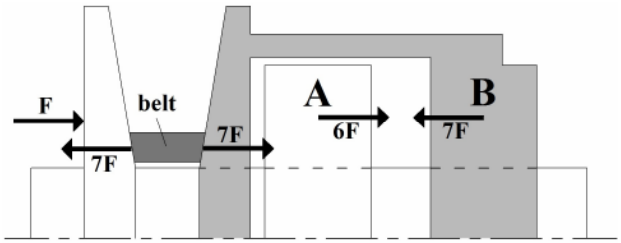

Fig. B.2. Representation of the force equilibrium on the assembled pulley shaft.

Figure B.3 and Fig. B.4 show the calculated stresses in the pulley shaft at a clamping force of 50 kN and a torque of 500 Nm. At a clamping force of 50 kN the shear force F_{sb} is approximately 2400 N and the force on the groove of the shaft is 43 kN. Because in working conditions the shaft is rotating, the direction of the shear force constantly changes. Because the slots in the shaft are considered to weaken the shaft, two situations are considered like indicated in the figures. It appears that the differences in the values of the stresses are rather small between the two situations. The maximum stress appears in the groove of the shaft, near the slot. The maximum value of the stress is rather large and would require the shaft to be made of a material with a very high yield stress. However, this stress peak appears to be very local and because of the extent of this research the design of the shaft is not completely optimized. Furthermore the results of FEM programs are very dependent of for instance the way the loads are applied, therefore they should always be critically analyzed.

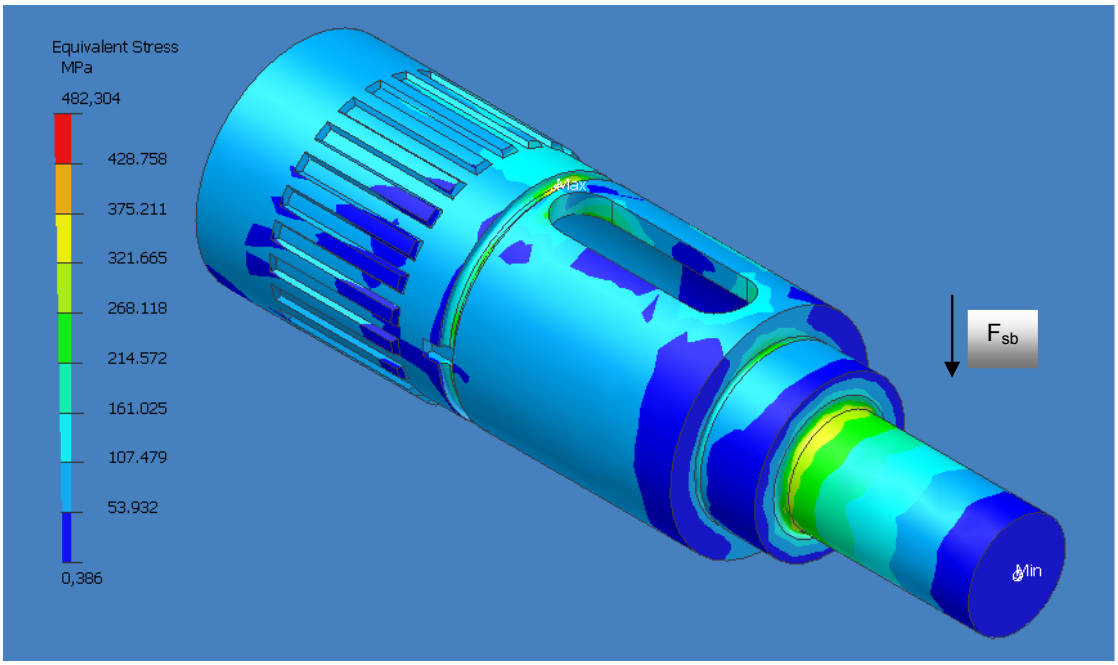

Fig. B.3. Stress distribution in the pulley shaft at a clamping force of 50 kN and a torque of 500 Nm, with the shear force F_{sb} acting downwards.

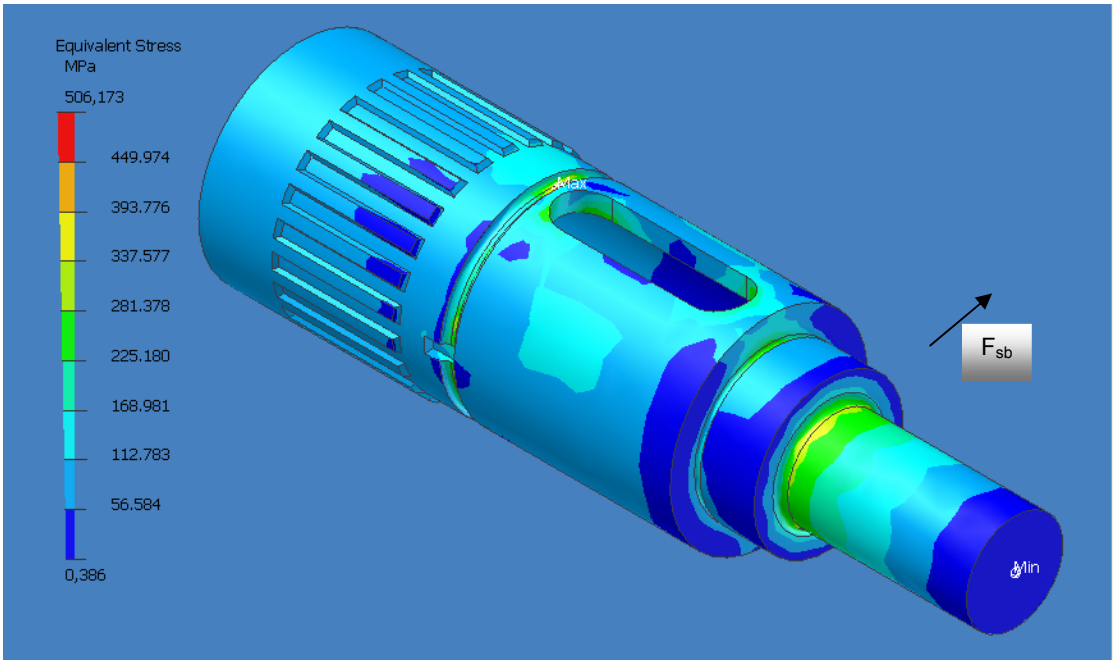

Fig. B.4. Stress distribution in the pulley shaft at a clamping force of 50 kN and a torque of 500 Nm, with the shear force F_{sb} acting from left to right.

B2. Roller system

The stresses in the rings of the roller system are also examined. Figure B.5 and Fig. B.6 show respectively the stresses in the fixed ring and the moveable ring at a clamping force of 50 kN. The maximum stress values are not problematic, and at some places with very low stresses material could be removed to reduce the weight of the rings.

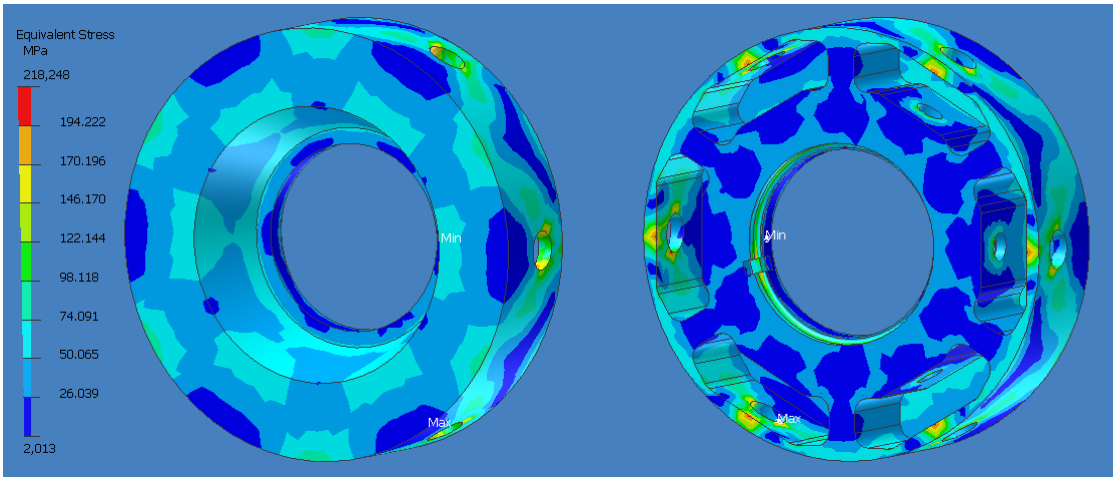

Fig. B.5. Stresses in fixed ring at clamping force of 50 kN.

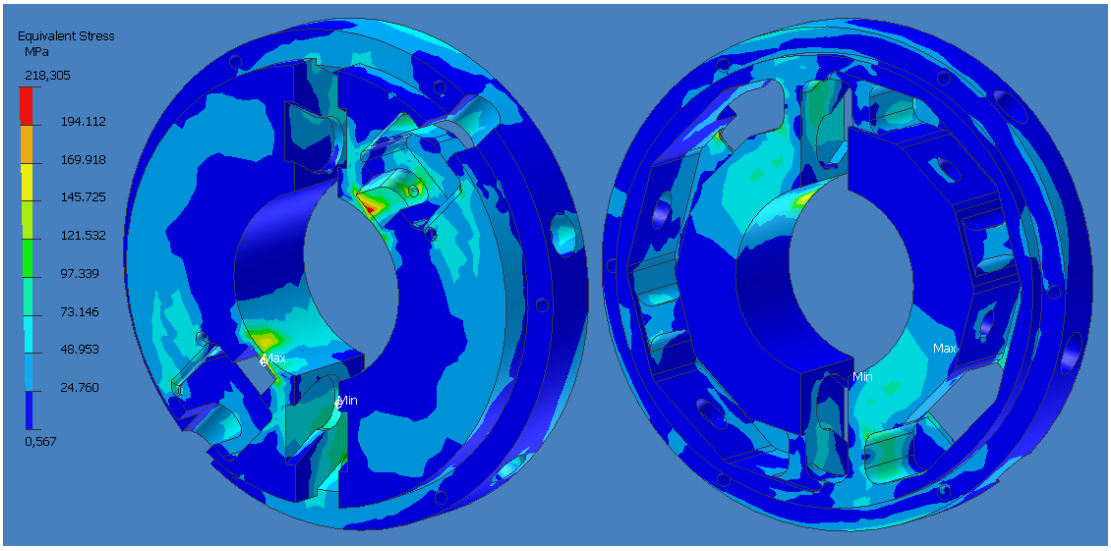

Fig. B.6. Stresses in moveable ring at clamping force of 50 kN.

APPENDIX C: MODELLING

C1. Rope model

To obtain an estimation of the friction losses inside the rope due to the bending while running over the rollers, a simplified model of the rope is considered, based on the figures below.

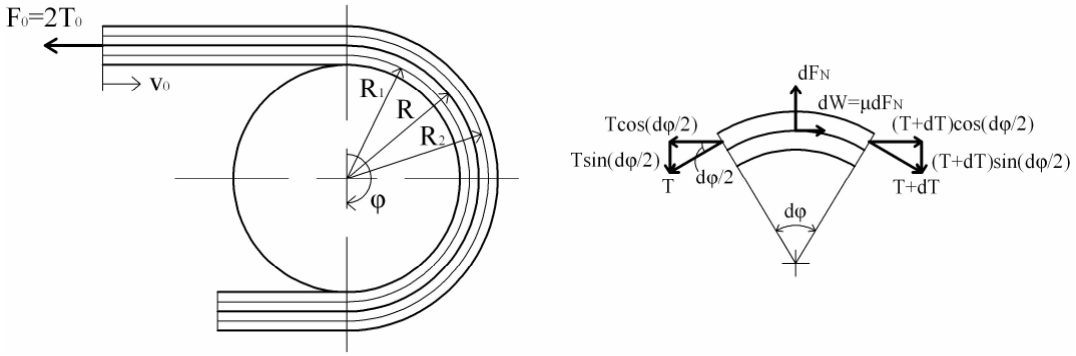

Fig. C.1. Representation of two-layer rope model.

The rope is assumed to consist of two layers, which slip along each other because of their different running radius over a roller. Although in reality the strands of the rope slide over each other in various directions, it is assumed this model gives a reasonable estimation of the friction losses inside the rope. The relative speed between the two layers equals:

$$v_{rel} = \left(\frac{R_2}{R} - \frac{R_1}{R}\right) \cdot v_0 \tag{C.1}$$

The right figure shows the forces acting on an element of the upper rope layer, which is assumed to slip over the lower layer with the relative speed. Summing the forces in vertical (radial) direction gives:

$$\begin{aligned} dF_N &= T \cdot \sin\left(\frac{d\varphi}{2}\right) + (T + dT) \cdot \sin\left(\frac{d\varphi}{2}\right) \\ &= (2T + dT) \cdot \sin\left(\frac{d\varphi}{2}\right) \end{aligned}$$

$dT << T$ And because $\frac{d\varphi}{2}$ is very small, $\sin\left(\frac{d\varphi}{2}\right) \approx \frac{d\varphi}{2}$. This results in:

$$dF_N = T \cdot d\varphi \tag{C.2}$$

Summing the forces in horizontal (tangential) direction gives:

$$\begin{aligned} T \cdot \cos\left(\frac{d\varphi}{2}\right) &= \mu \cdot dF_N + (T + dT) \cdot \cos\left(\frac{d\varphi}{2}\right) \\ \mu \cdot dF_N + dT \cdot \cos\left(\frac{d\varphi}{2}\right) &= 0 \end{aligned}$$

Because $\frac{d\varphi}{2}$ is very small, $\cos\left(\frac{d\varphi}{2}\right) \approx 1$. This results in:

$$-\mu \cdot dF_N = dT \tag{C.3}$$

With μ [-] the coefficient of friction between the layers. SubstitutingEq. (C.2) in Eq. (C.3) gives:

$$-\mu \cdot d\varphi = \frac{dT}{T} \tag{C.4}$$

Integrating Eq. (C.4) gives:

$$-\mu \cdot \int_0^{\varphi} d\varphi = \int_{T_0}^{T_1} \frac{1}{T}\, dT$$

$$-\mu \cdot \varphi = \ln\left(\frac{T_1}{T_0}\right)$$

$$\frac{T_1}{T_0} = e^{-\mu\varphi}$$

For the tensile force *T(φ)* in the upper rope layer this results in:

$$T(\varphi) = T_0 \cdot e^{-\mu\varphi} \tag{C.5}$$

Where T_0 is the initial tensile force in the upper layer of the straight part. The frictional power loss inside the rope and the efficiency of the rope when moving over one roller can now be estimated with:

$$\begin{aligned} P_{loss} &= (T_0 - T(\varphi)) \cdot v_{rel} \\ &= T_0 \cdot v_0 \cdot \left(1 - e^{-\mu\varphi}\right) \cdot \left(\frac{R_2}{R} - \frac{R_1}{R}\right) \end{aligned} \tag{C.6}$$

$$\begin{aligned} \eta &= \frac{P_{in} - P_{loss}}{P_{in}} \\ &= \frac{2T_0 \cdot v_0 - P_{loss}}{2T_0 \cdot v_0} \\ &= 1 - \frac{1}{2} \cdot \left(1 - e^{-\mu\varphi}\right) \cdot \left(\frac{R_2}{R} - \frac{R_1}{R}\right) \end{aligned} \tag{C.7}$$

In the roller system, the contact angle between the rope and the rollers $\varphi = \pi$ [rad]. The estimated coefficient of friction between the layers (Technora) $\mu \approx 0.15$ [-]. This results in a power loss and rope efficiency over a roller with tread diameter of 24 mm of:

$$\begin{aligned} \eta &= 1 - \frac{1}{2} \cdot \left(1 - e^{-0.15 \cdot \pi}\right) \cdot \left(\frac{14.25}{13.5} - \frac{12.75}{13.5}\right) \\ &\approx 0.979 \end{aligned}$$

C2. Total roller system model

Besides the internal rope friction, the total Matlab/Simulink model also calculates the friction losses of the rollers and the friction loss of the sliding contact between the moveable ring and the pulley shaft. The rollers are made of rolling bearings which makes it possible to use standard bearing friction equations as defined by bearing manufacturers. The friction force F_w [N] between the moveable ring and the pulley shaft is calculated with:

$$F_w = \mu_R \cdot F_N \tag{C.8}$$

Where μ_R is the friction coefficient between the moveable ring and the shaft and F_N is the normal force on the contact surface, in this case the weight of the moveable ring.

If a rotating pulley shaft is considered, the frictional forces between the rollers and the Teflon rings due to the centrifugal force should also be modelled.

APPENDIX D: TEST SET-UP

D1. Test construction

The part of the new CVT actuation system design that is manufactured for the test set-up is shown in Fig. D.1. To reduce the manufacturing time, costs and complexity, it was chosen to use a non-rotating shaft without the extra roller system and thrust bearing inside the shaft. The set-up is used to test the working principle of the roller system and to measure its efficiency.

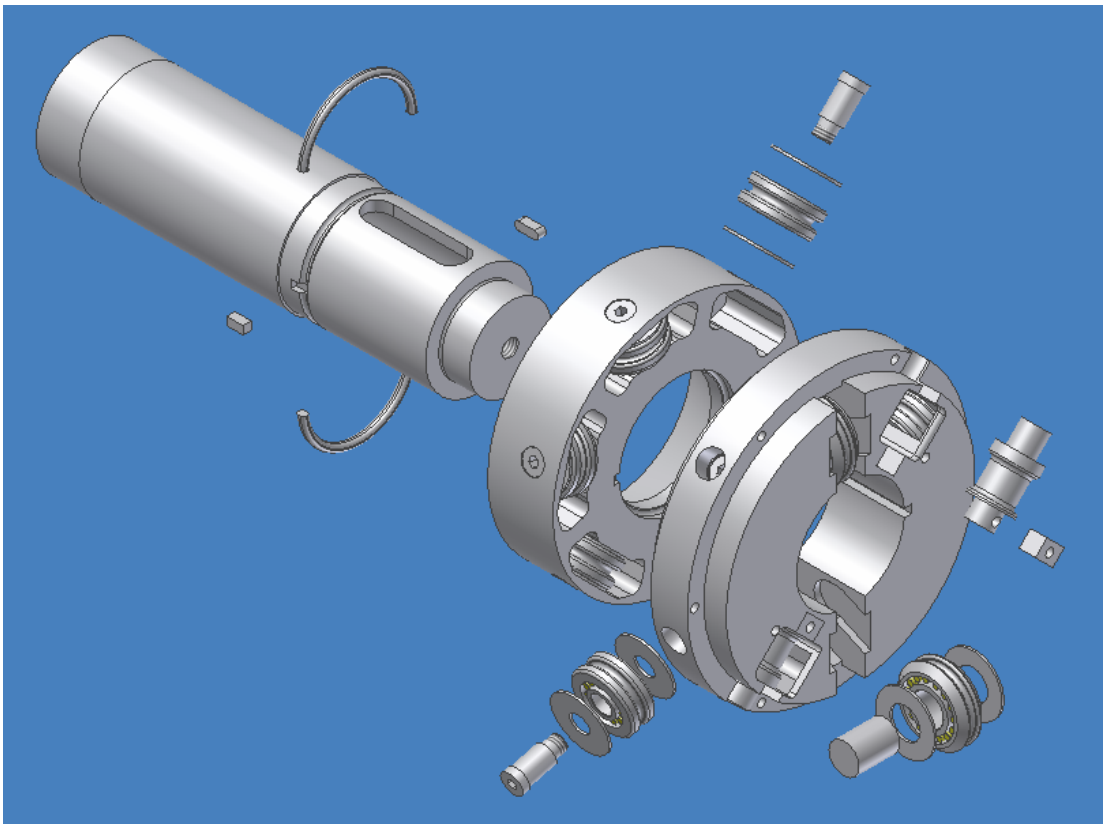

Fig. D.1. Manufactured test construction.

D2. Total test setup

A picture of the total test setup that is used for the efficiency measurements is shown in Fig. D.2. The actuation shaft with the drum in the lower part of the picture is designed by another student. To drive the actuation shaft a hydraulic motor is connected to it, and sensors are added to measure the rotational speed and the torque. The rest of the test setup is designed to be able to measure the output force of the roller system and at the same time providing a counterforce for it. Furthermore the outgoing speed of the roller system is measured.
With use of the hydraulic motor a sinusoidal input speed is generated while applying a constant input torque. By winding and unwinding the rope loop on the drum with the input speed under the input torque, the roller system is actuated. The hydraulic cylinder provides a constant counterforce for the roller system. The actuation torque T_{act} [Nm] is measured with a torque sensor and the angular speed of the drum ω_{drum} [rad/s] is obtained by differentiating the signal of a rotary encoder fixed to the actuation shaft. The output force F_{clamp} [N] is measured with a load cell and the speed of the moveable ring v_{ring} [m/s] is obtained by differentiating the signal of a digital length gauge that measures the slider ring position.
Figure D.3 and Fig. D.4 show CAD drawings of the designed test set-up construction. The dark grey parts are standard parts that were already available, the light grey parts are specially designed and manufactured for the test set-up.

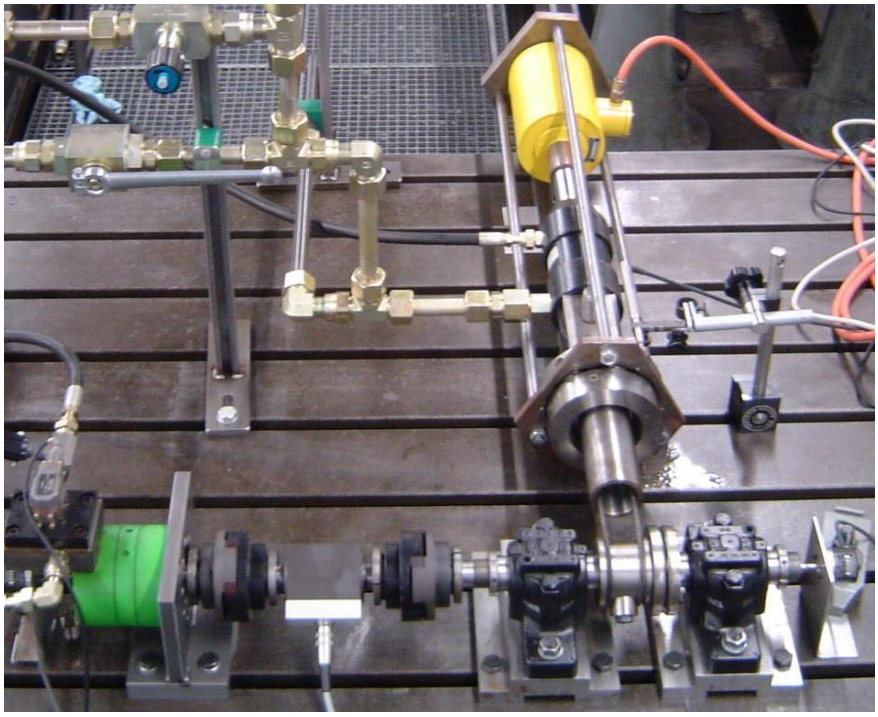

Fig. D.2. The test setup.

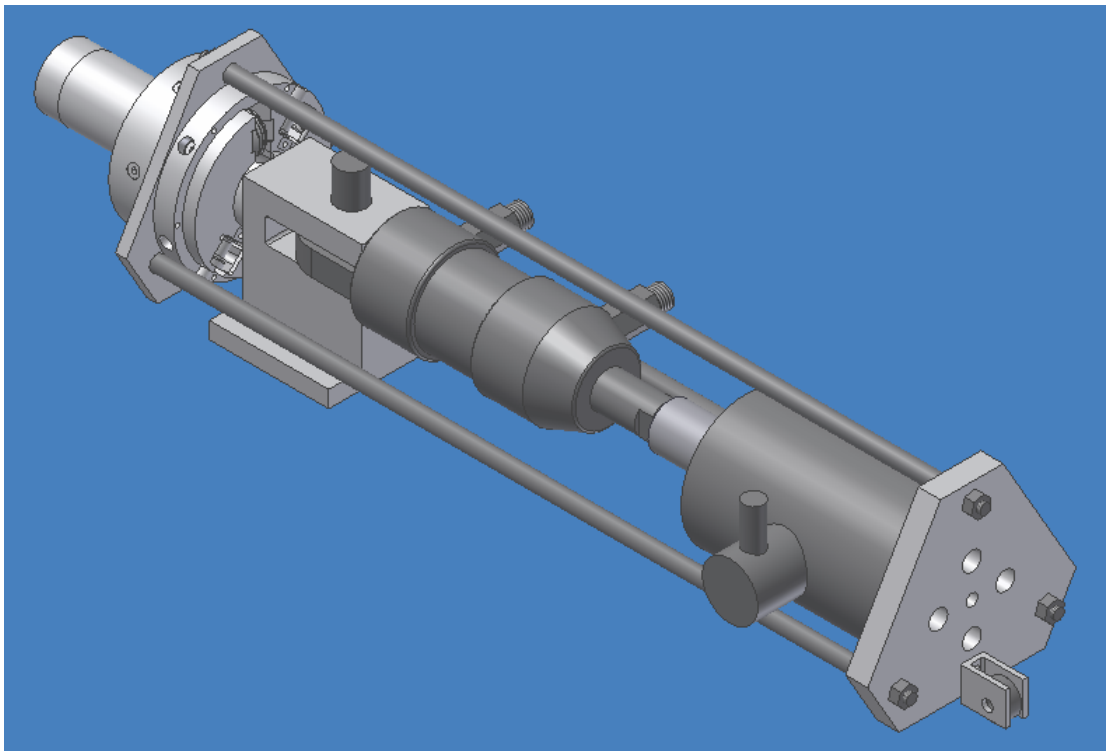

Fig. D.3. CAD drawing of part of the test setup.

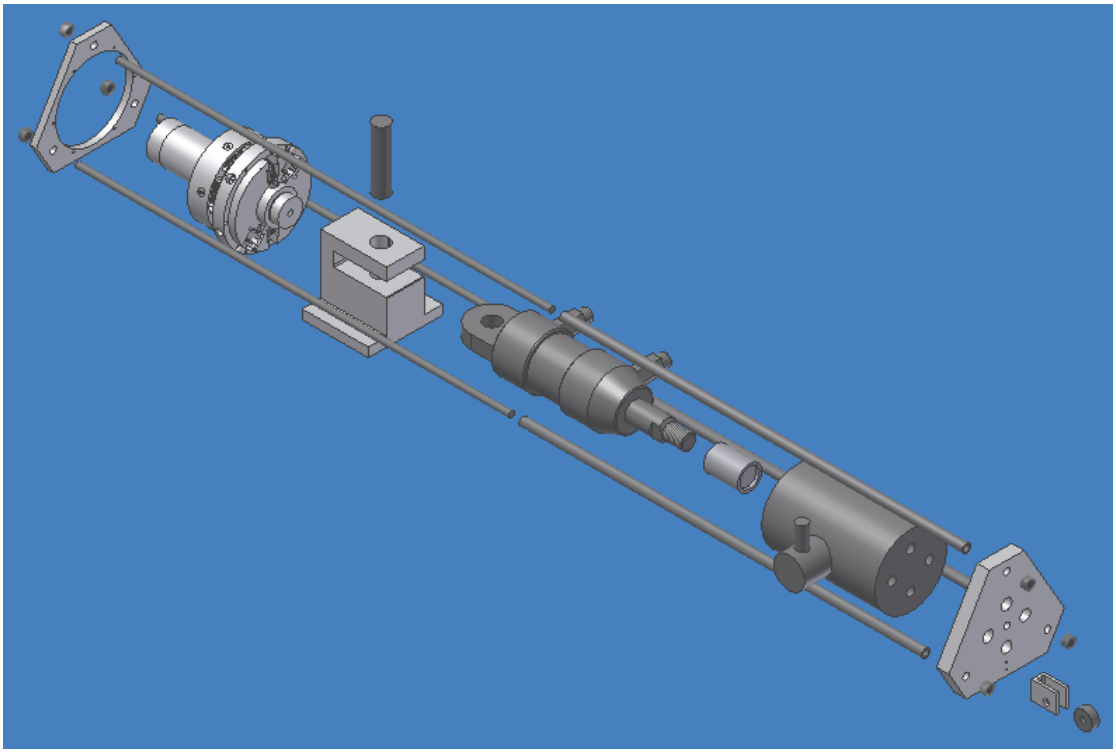

Fig. D.4. Exploded view of the parts of the test set-up.

D3. Sensor specifications

Torque sensor
Manufacturer: HBM
Type: T20WN / 200Nm
Resolution: 0.4 Nm (0.2 % of nominal torque)
Sensitivity: 0.05 V/Nm
Zero drift: +/- 0.2 V

Rotary encoder
Manufacturer: Heidenhain
Type: ROD 1020
Resolution: 0.025° ($4.4*10^{-4}$ rad)
Sensitivity: 14400 pulses/revolution

Load cell
Manufacturer: HBM
Type: C3
Resolution: 100 N (after calibration, see Fig. D.5)
Sensitivity: 0.0001 V/N (after calibration, see Fig. D.5)

Digital length gauge
Manufacturer: Heidenhain
Type: SPECTO ST 3078
Resolution: 1 m
Sensitivity: 1000 pulses/mm

kN	V
0,00	0,00
5,02	0,50
8,06	0,80
12,94	1,29
18,44	1,84
25,85	2,58
35,50	3,55
46,05	4,61
57,10	5,71
59,62	5,96
46,10	4,61
37,96	3,80
31,50	3,15
18,52	1,85
8,86	0,89
0,00	0,00

measurement range 1mV/V
calibration signal 4.91V

amplifier HBM type KWS 503A / D93737
load cell HBM C3 FNr.25189

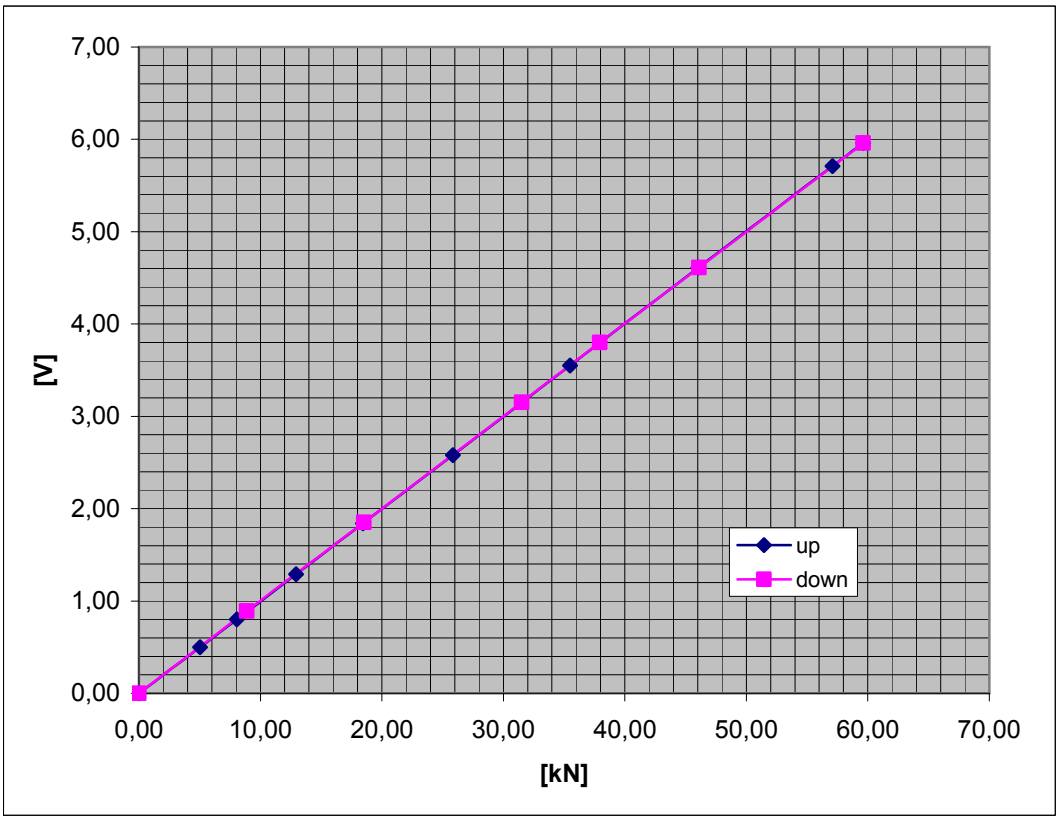

Fig. D.5. Load cell calibration sheet.

APPENDIX E: ROLLER SYSTEM EFFICIENCY

In this appendix the roller system efficiency measurement results are presented and compared with the roller system model. Furthermore the measurement accuracy is estimated.

E1. Measurement results

Figure E.1a shows the relation between the actuation force, calculated from the actuation torque and the radius on which the rope loop is winded around the drum, and the actual clamping force. The two depicted measurements are performed with different actuation speeds. The figure shows measurement points at moveable ring speeds of 14 and 28 mm/s. Figure E.1b shows the roller system efficiency from the same measurements, calculated with:

$$\eta = \frac{P_{out}}{P_{in}} = \frac{F_{clamp} \cdot v_{ring}}{T_{act} \cdot \omega_{drum}} \tag{E.1}$$

Where P_{in} [W] and P_{out} [W] are respectively the input power and the output power of the roller system. It appears that the actuation speed does not have a significant influence on the roller system efficiency.

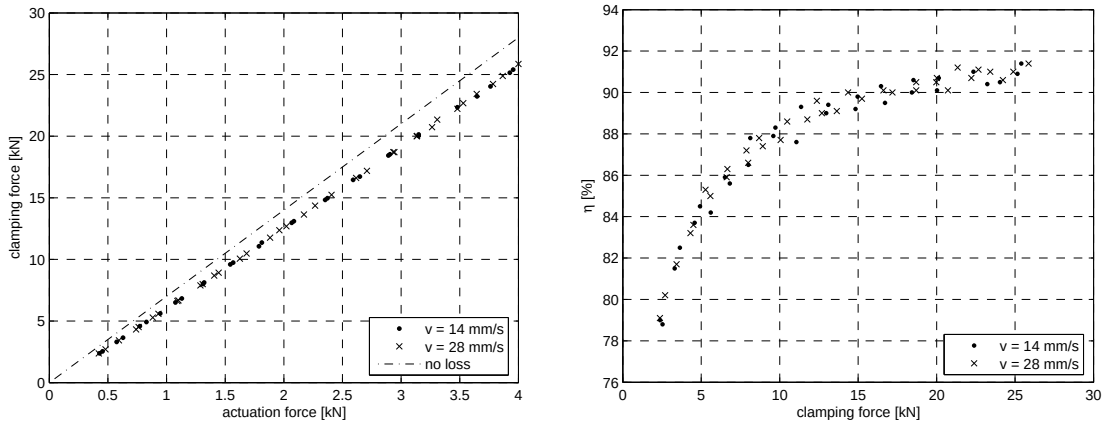

Fig. E.1. Efficiency measurement results at different speeds of the moveable ring.

Figure E.2 shows the relation between the actuation force and the clamping force for three independent measurements, which all nearly show the same results. It appears that this relation can be approximated with a linear fit:

$$F_{clamp} = c \cdot F_{act} + F_{clamp,0} \tag{E.2}$$

This indicates that the losses in the system consist of a constant part with value $F_{clamp,0}/c$, and a part that is dependent on the clamping force. Because of the transmission ratio i [-] of seven, in theory, the clamping force is seven times the actuation force (no loss).

$$F_{clamp,th} = i \cdot F_{act} \tag{E.3}$$

The system efficiency can now be estimated with use of Eq. (E.2) and Eq. (E.3) by:

$$\eta_{est} = \frac{F_{clamp}}{F_{clamp,th}} \tag{E.4}$$

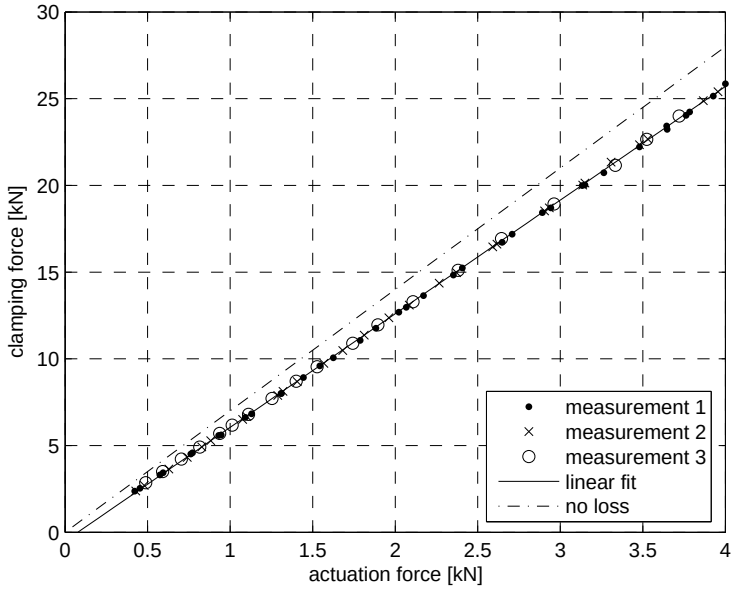

Fig. E.2. Relation between actuation force and clamping force.

Figure E.3 shows the estimated efficiency derived from the linear fit, together with the efficiency calculated from the measurement data by Eq. (E.1). It appears that the linear relation of Eq. (E.2) gives a good estimate of the roller system efficiency. Only at clamping forces below 5 kN the differences with the measured efficiency become rather large.

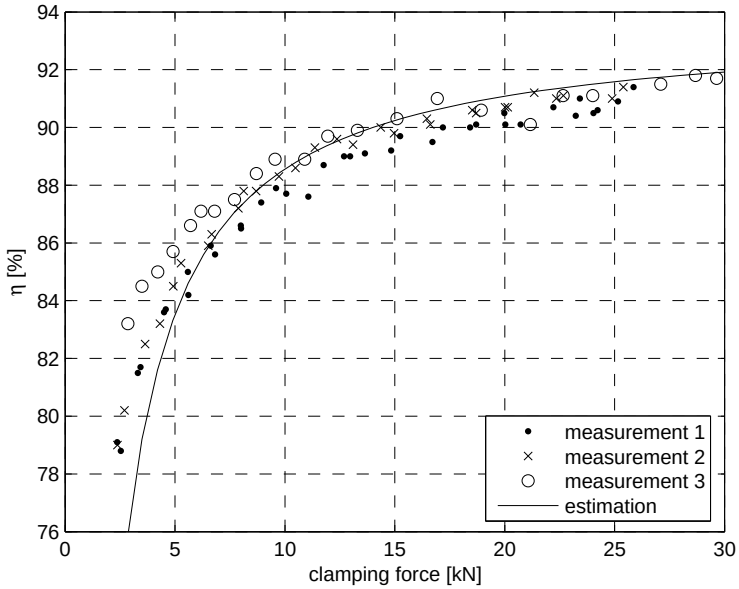

Fig. E.3. Roller system efficiency measurement results compared with the estimated efficiency derived from Eq. (E.2).

Figure E.4 shows the efficiency predicted by the Matlab/Simulink computer model compared to the measurement results. It appears that the model results do not correspond to the measurement data very well. It seems that an additional friction loss is present in the roller system, which is not included in the model. This additional friction loss is assumed to be mainly caused by the unexpected considerable friction force between the rope and the rollers. This friction initially was not included in the model because it is very difficult to estimate, and the slip between the rope and the rollers was assumed to be

very small. Furthermore this friction could explain the failure of the rope that occurred during the measurements, which was clearly caused by wear of the rope.
The rope specifications state a rope diameter of 3 mm. The actual rope diameter appears to be somewhat larger, especially at small rope loads. The grooves in the outer rings of the rollers however are designed assuming a rope diameter of 3 mm. Furthermore the grooves have rather steep sides, like shown in Fig. E.5a. Because of the larger rope diameter and the shape of the grooves, the rope gets clamped inside the groove. Especially when entering and leaving the roller, this can cause significant friction between the rope and the roller groove sides. Adding a constant friction force at each roller improves the model significantly. The efficiency predicted by the adjusted model with an additional friction force of 13 N at each roller is also plotted in Fig. E.4.

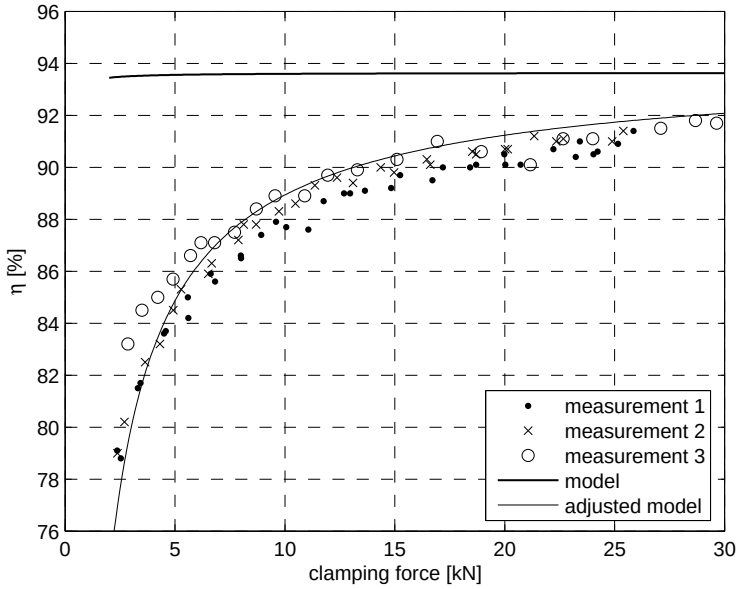

Fig. E.4. Efficiency predicted by the original Matlab/Simulink model and the adjusted model compared with the measurement results.

Assuming that the friction between the rope and the rollers is the real cause of the difference in efficiency, it is proposed to adjust the grooves of the rollers to a shape more like shown in Fig. E.5b. This groove shape is assumed to decrease the friction between the rope and the rollers, which can significantly improve the roller system efficiency and diminish the wear of the rope. It is however recommended to examine the relation between the shape of the groove, the roller system efficiency and the wear of the rope before adjusting the grooves.

Fig. E.5. a) Initial roller groove shape. b) Proposed adjusted roller groove shape.

E2. Measurement accuracy

To give an indication of the accuracy of the measurements, an error budget has been formed. To calculate the uncertainty in the measured roller system efficiency, all the uncertainties of the variables in the calculation of the efficiency have to be estimated. The efficiency η [%] is calculated from the measurement data with:

$$\eta = \frac{F_{clamp} \cdot v_{ring}}{T_{act} \cdot \omega_{drum}} \cdot 100\% \qquad \text{(E5)}$$

The uncertainty of the clamping force F_{clamp} is estimated to be equal to the resolution of the load cell, which is 100 N. For the estimation of the uncertainty of the ring speed v_{ring} it is assumed that this uncertainty is caused by the digital length gauge being not placed precisely at right angles to the moveable ring of the roller system. A maximum deviation of 2° is assumed which causes a maximum deviation of the measured position of 7 m. When a squared distribution of the error is assumed, the uncertainty of the ring speed equals 7/√3 ≈ 4 m/s. The uncertainty of the torque T_{act} is assumed to be caused by the zero drift of the torque sensor. The maximum zero drift equals 0.2 V according to the specifications, which equals 4 Nm. When again a squared distribution of the error is assumed this results in an uncertainty of 4/√3 ≈ 2.3 Nm. The uncertainty of the angular speed of the drum ω_{drum} is estimated to be equal to the resolution of the rotary encoder, which results in an uncertainty of 0.00044 rad/s.

Table E.1.
Error budget for the calculation of the roller system efficiency from the measurement data.

VARIABLE	VALUE x_i	ESTIMATED UNCERTAINTY u_i	SENSITIVITY COEFFICIENT $c_i = \frac{\partial \eta}{\partial x_i}$	CONTRIBUTION TO UNCERTAINTY IN η $c_i \cdot u_i$
F_{clamp}	15069 N	100 N	0.00602 %/N	0.602 %
v_{ring}	0.0271 m/s	4 m	3347 %s/m	0.013 %
T_{act}	74.457 Nm	2.3 Nm	1.218 %/Nm	2.80 %
ω_{drum}	6.047 rad/s	0.00044 rad/s	15.0 %s/rad	0.0066 %
η	**90.70 %**			**2.9 %**

The error budget of one measurement point at a clamping force of approximately 15 kN is presented in Table E1. The resulting uncertainty of the measured roller system efficiency is about 3 %, which means that the real efficiency at a clamping force of 15 kN is assumed to be between 87.7 % and 93.7 %.

APPENDIX F: ESTIMATE OF ROLLER SYSTEM COSTS

A rough estimate of the roller system costs of one pulley shaft is made, which include the rings that contain the rollers, the rollers, the roller axles, the Teflon rings, the drum axles with fix blocks and the rope and the thrust bearing inside the pulley shaft.

Roller system rings
The two rings of the roller system that contain the rollers are made of 34CrNiMo6 steel, which costs about 4,- €/kg. The weight of the total material needed for manufacturing the rings is about 8 kg, which results in the material costs of about € 32,-.

Rollers
The rollers are made of rolling bearings, type STO 10 and STO 15 which cost about € 31,- and € 34,- respectively. For the roller system of one pulley shaft, ten STO 10 bearings and two STO 15 bearings are needed. This results in the total costs of about 380,-.

Roller axles
The roller axles are made of 34CrNiMo6 steel and have a total weight of about 0.3 kg, which results in the total costs of about € 1,20

Teflon rings
For the Teflon rings about 0.022 m^2 of Teflon with a thickness of 1 mm is needed, which costs about 230 €/m^2. This results in the total costs of about € 5,-.

Drum axles & fix blocks
The drum axles and fix blocks are also made of 34CrNiMo6 steel. Because of their low weight the material costs are negligible.

Rope
The 3 mm (1/8”) Tech 12 rope costs about € 1,10 per meter. Only a few meters of rope are needed for the roller system.

Thrust bearing
The thrust bearing type 51202 costs about € 19,-.

The total material costs of the roller system of one pulley shaft is about € 450,-. The working hours needed to manufacture the various parts are estimated to be about 150 hours. It should be remarked that the total costs to manufacture a roller system in large scale production will be considerably lower.

APPENDIX G: CONSTRUCTION DRAWINGS

This appendix contains all the construction drawings for manufacturing the test construction shown in the figure below. The drawings are presented in the order of the numbers in the figure:

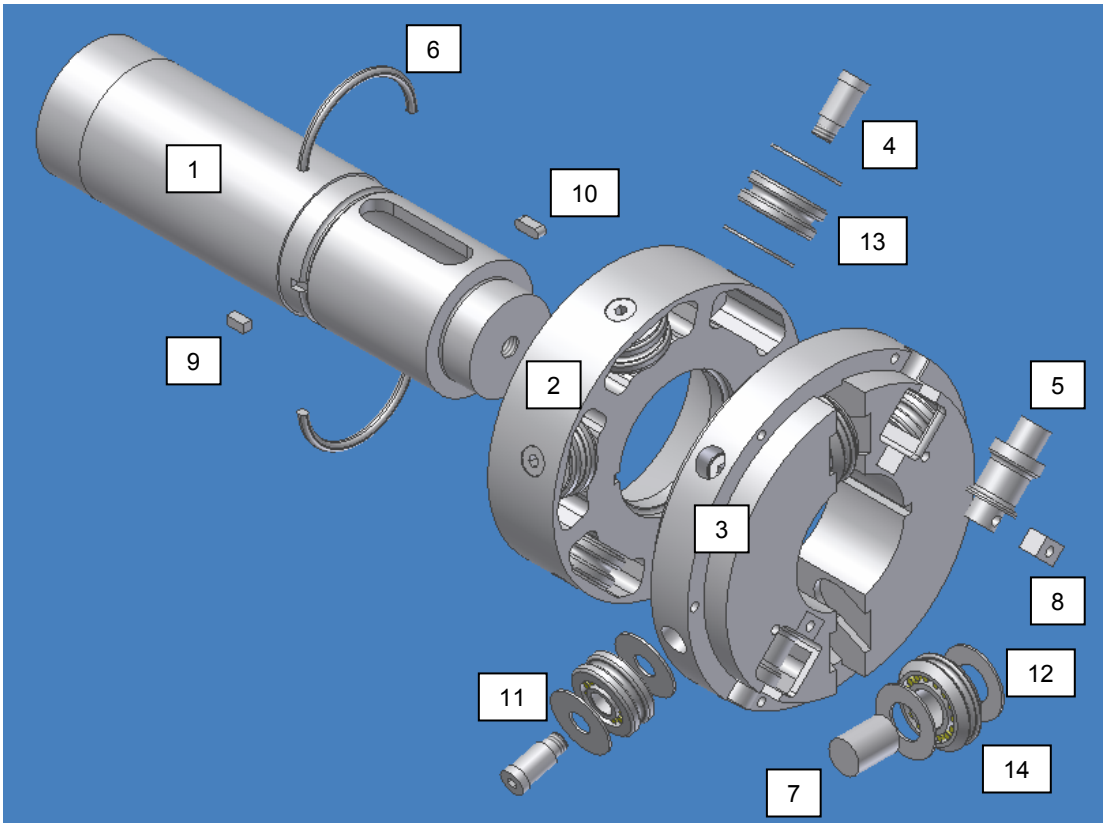

Fig. F.1. Exploded view of the manufactured test construction.

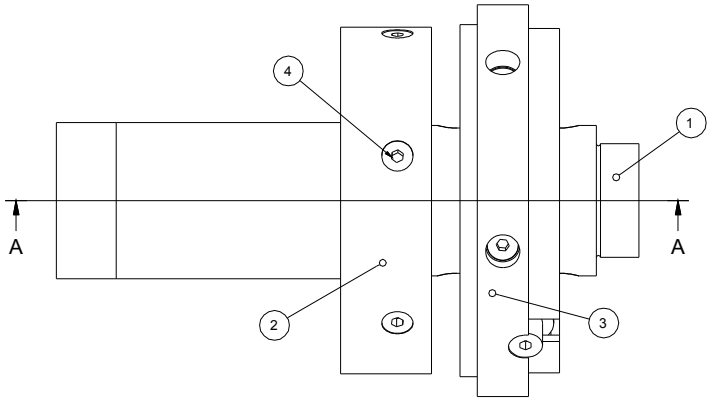

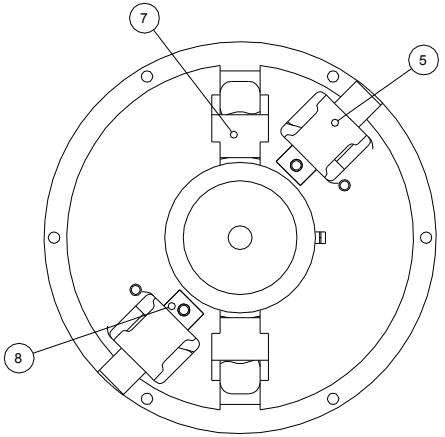

A-A (1 : 1)

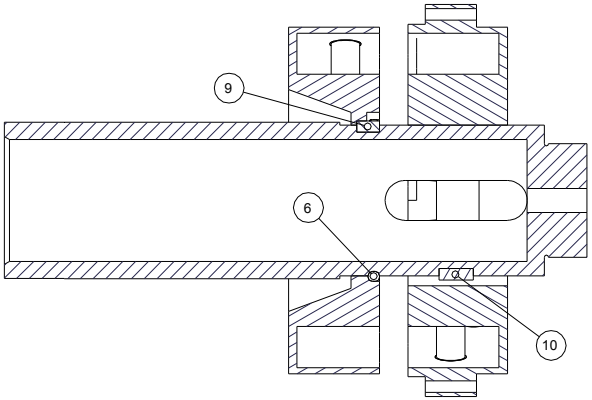

Parts List					
POS.	BENAMING	AANT	TEK.NR.	MATERIAAL	OPMERKINGEN
1	Shaft	1	TEK.1	34CrNiMo6	
2	Shaft Ring	1	TEK.2	34CrNiMo6	
3	Slider Ring	1	TEK.3	34CrNiMo6	
4	Pin	10	TEK.4	34CrNiMo6	
5	Drum Axis	2	TEK.5	34CrNiMo6	
6	Ring	2	TEK.6	34CrNiMo6	
7	Axls_15	2	TEK.7	34CrNiMo6	
8	Fix Block	2	TEK.8	34CrNiMo6	
9	Key1	1	TEK.9		te maken van bijgeleverde sple
10	Key2	1	TEK.10		bijgeleverd

TOLERANTIES VOLGENS NEN 2365
B.V. tot 1 | ± 30' | ± 30 ''
PASSINGEN VOLGENS N802 | RUWHEIDSWAARDEN VOLGENS NEN630

PROJECTIE

BENAMING:
Assembly
Pulley Concept CVT

AANTAL: 1 | MATERIAAL: 34CrNiMo6

Technische Universiteit Eindhoven
TU/e

SCHAAL: 1:1 | DATUM: 2/23/2005 | TEKENINGNR: Assembly | A2
GET.: R. Drabbels
TELNR: 2771
REVISIE

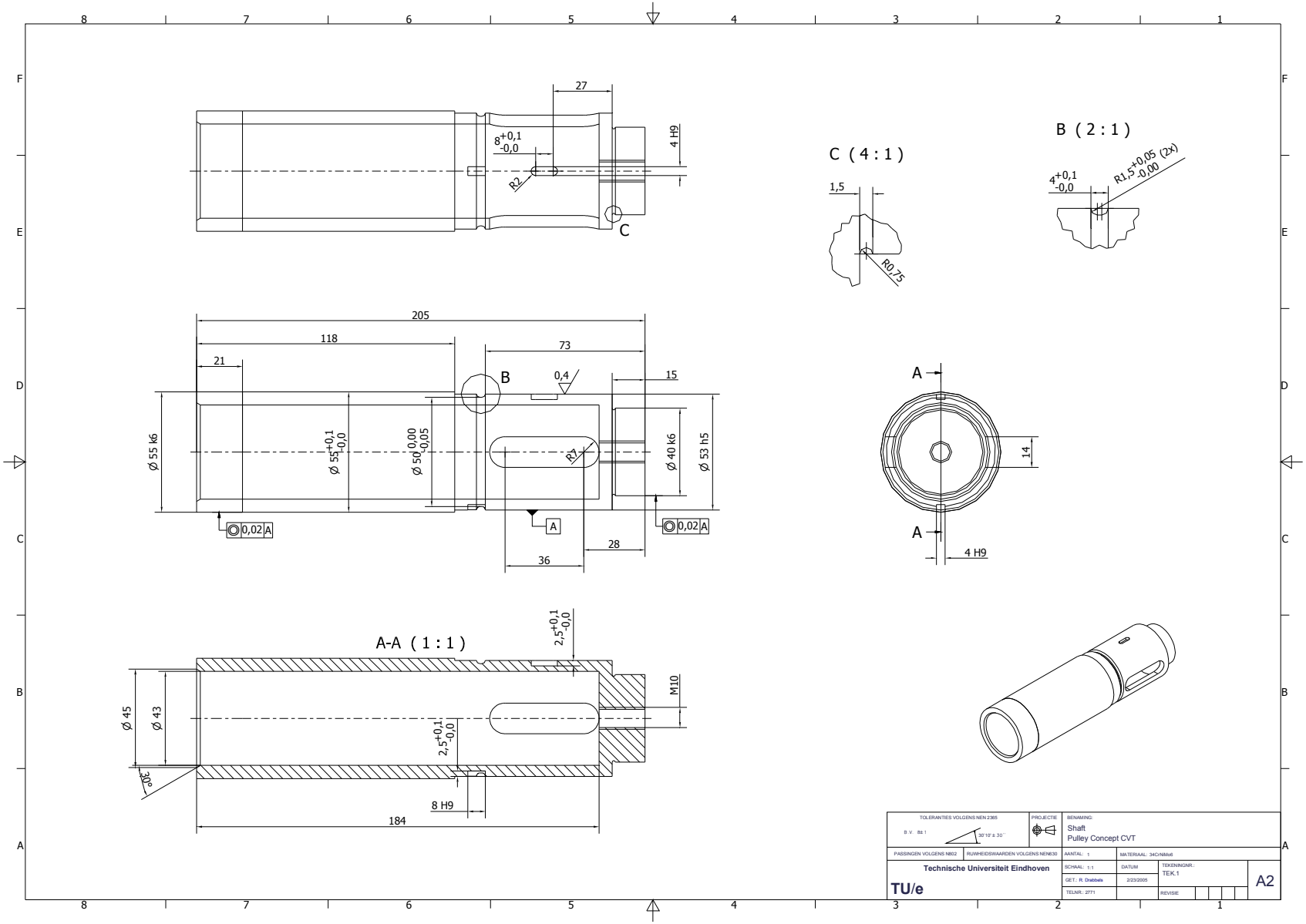

TOLERANTIES VOLGENS NEN 2365 B.V. 8± 1 ∠ 30' 10' ± 30''	PROJECTIE	BENAMING: Shaft Pulley Concept CVT
PASSINGEN VOLGENS N802	RUWHEIDSWAARDEN VOLGENS NEN630	AANTAL: 1
		MATERIAAL: 34Cr/NiMo6
Technische Universiteit Eindhoven		SCHAAL: 1:1
TU/e		DATUM: 2/23/2005
		TEKENINGNR.: TEK.1
		GET.: R. Drabbels
		TELNR.: 2771
		REVISIE
		A2

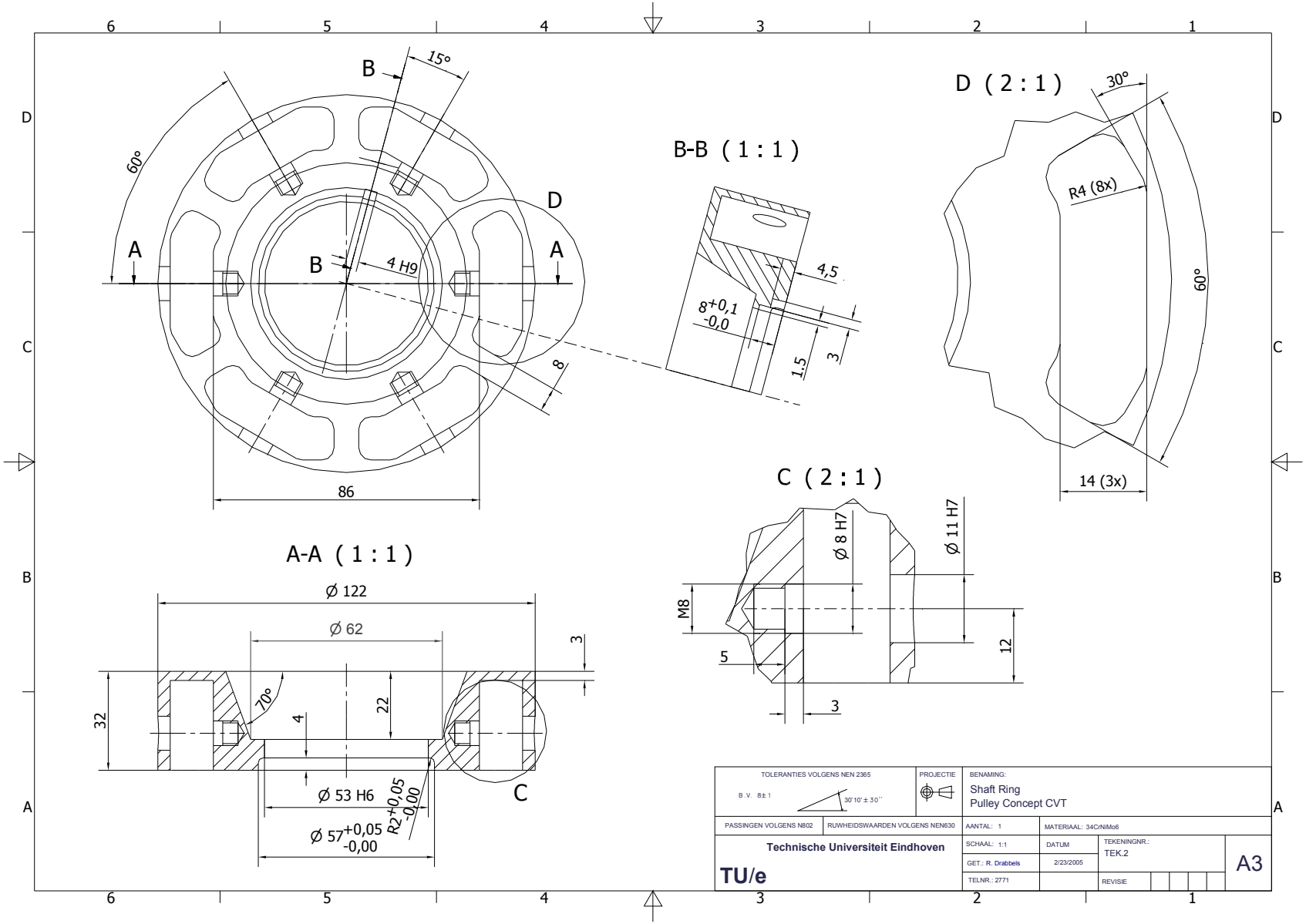
B
15°
60°
A
B
4 H9
D
A
8
86
B-B (1 : 1)
4,5
8+0,1 -0,0
1,5
3
D (2 : 1)
30°
R4 (8x)
60°
14 (3x)
C (2 : 1)
Ø 8 H7
Ø 11 H7
M8
5
12
3
A-A (1 : 1)
Ø 122
Ø 62
3
32
70°
4
22
Ø 53 H6
R2+0,05 -0,00
Ø 57+0,05 -0,00
C
TOLERANTIES VOLGENS NEN 2365
B.V. 8± 1
30' 10' ± 30''
PROJECTIE
BENAMING:
Shaft Ring
Pulley Concept CVT
PASSINGEN VOLGENS N802
RUWHEIDSWAARDEN VOLGENS NEN630
AANTAL: 1
MATERIAAL: 34CrNiMo6
Technische Universiteit Eindhoven
TU/e
SCHAAL: 1:1
DATUM
TEKENINGNR.:
TEK.2
GET.: R. Drabbels
2/23/2005
A3
TELNR.: 2771
REVISIE

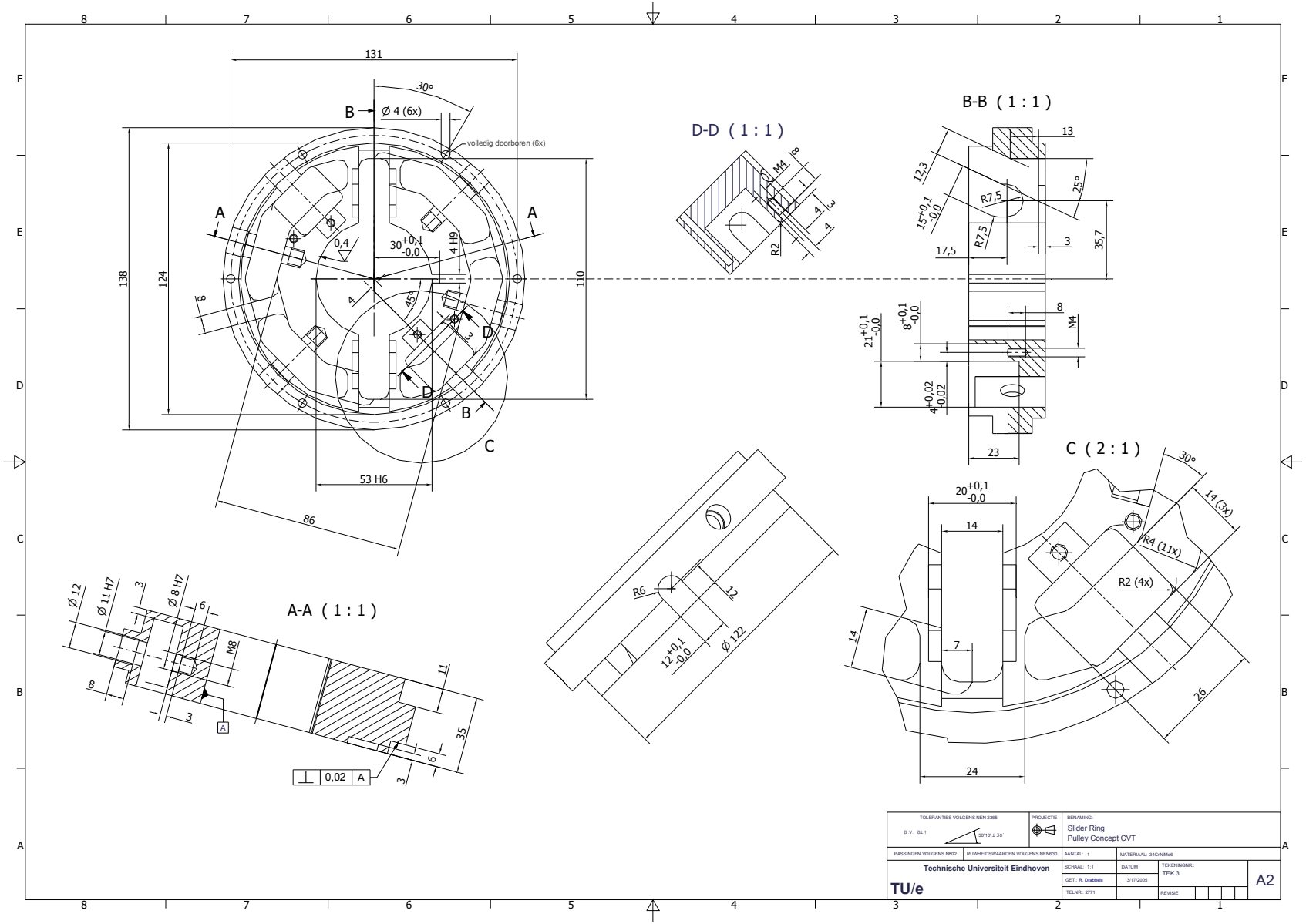
131
30°
B
Ø 4 (6x)
volledig doorboren (6x)
A
A
0,4
30+0,1 -0,0
4 H9
138
124
8
4
45°
110
D
D
B
C
53 H6
86
D-D (1 : 1)
M4
8
4
3
4
R2
B-B (1 : 1)
13
12,3
25°
15+0,1 -0,0
R7,5
R7,5
17,5
3
35,7
21+0,1 -0,0
8+0,1 -0,0
8
M4
4+0,02 -0,02
23
C (2 : 1)
30°
14 (3x)
20+0,1 -0,0
14
R4 (11x)
R2 (4x)
14
7
26
24
A-A (1 : 1)
Ø 12
Ø 11 H7
3
Ø 8 H7
6
M8
8
3
A
11
35
6
3
0,02 A
R6
12
12+0,1 -0,0
Ø 122
TOLERANTIES VOLGENS NEN 2365
B.V. Bd.1
30' 10' ± 30''
PROJECTIE
BENAMING:
Slider Ring
Pulley Concept CVT
PASSINGEN VOLGENS N802
RUWHEIDSWAARDEN VOLGENS NEN630
AANTAL: 1
MATERIAAL: 34CrNiMo6
Technische Universiteit Eindhoven
TU/e
SCHAAL: 1:1
DATUM
TEKENINGNR:
TEK.3
GET.: R. Drabbels
3/17/2005
A2
TELNR.: 2771
REVISIE

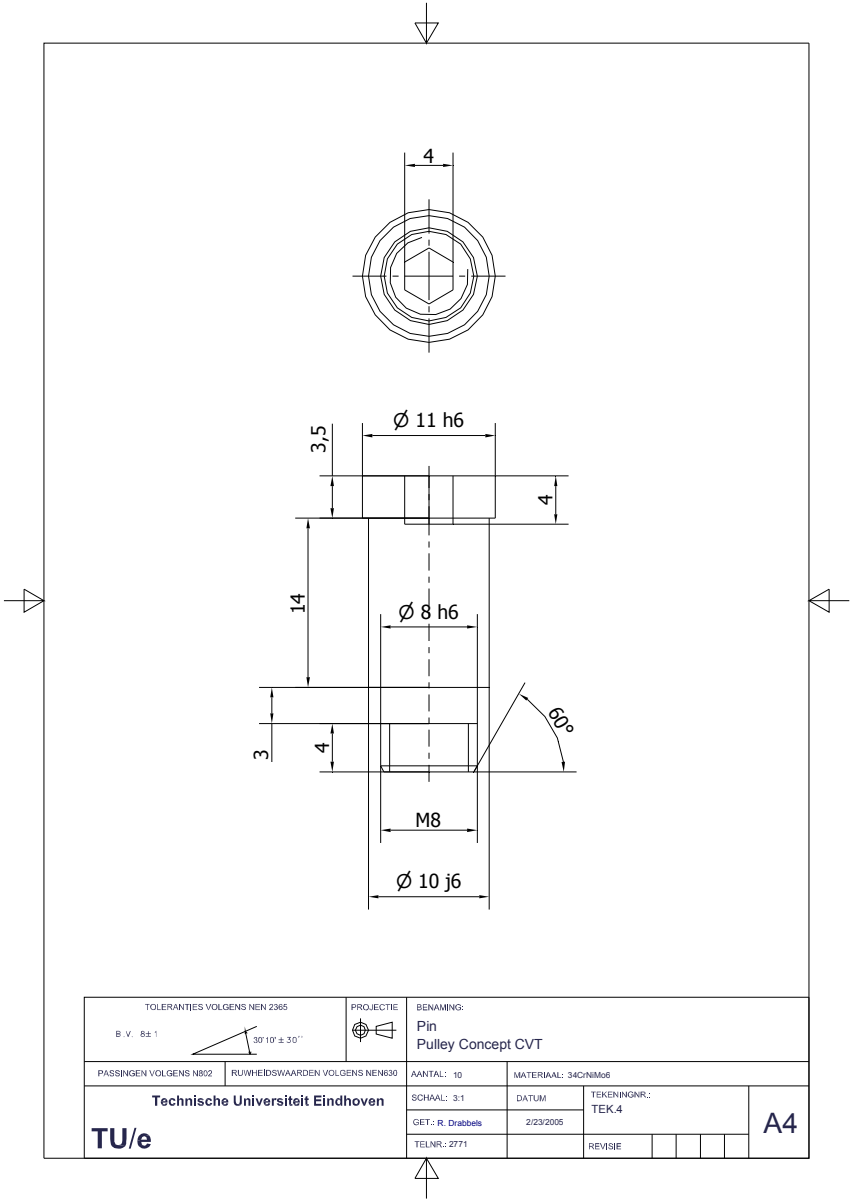

TOLERANTIES VOLGENS NEN 2365 B.V. 8± 1 30'10' ± 30''	PROJECTIE	BENAMING: Pin Pulley Concept CVT	
PASSINGEN VOLGENS N802	RUWHEIDSWAARDEN VOLGENS NEN630	AANTAL: 10	MATERIAAL: 34CrNiMo6
Technische Universiteit Eindhoven TU/e		SCHAAL: 3:1 / GET.: R. Drabbels / TELNR.: 2771	DATUM: 2/23/2005 / REVISIE
		TEKENINGNR.: TEK.4	A4

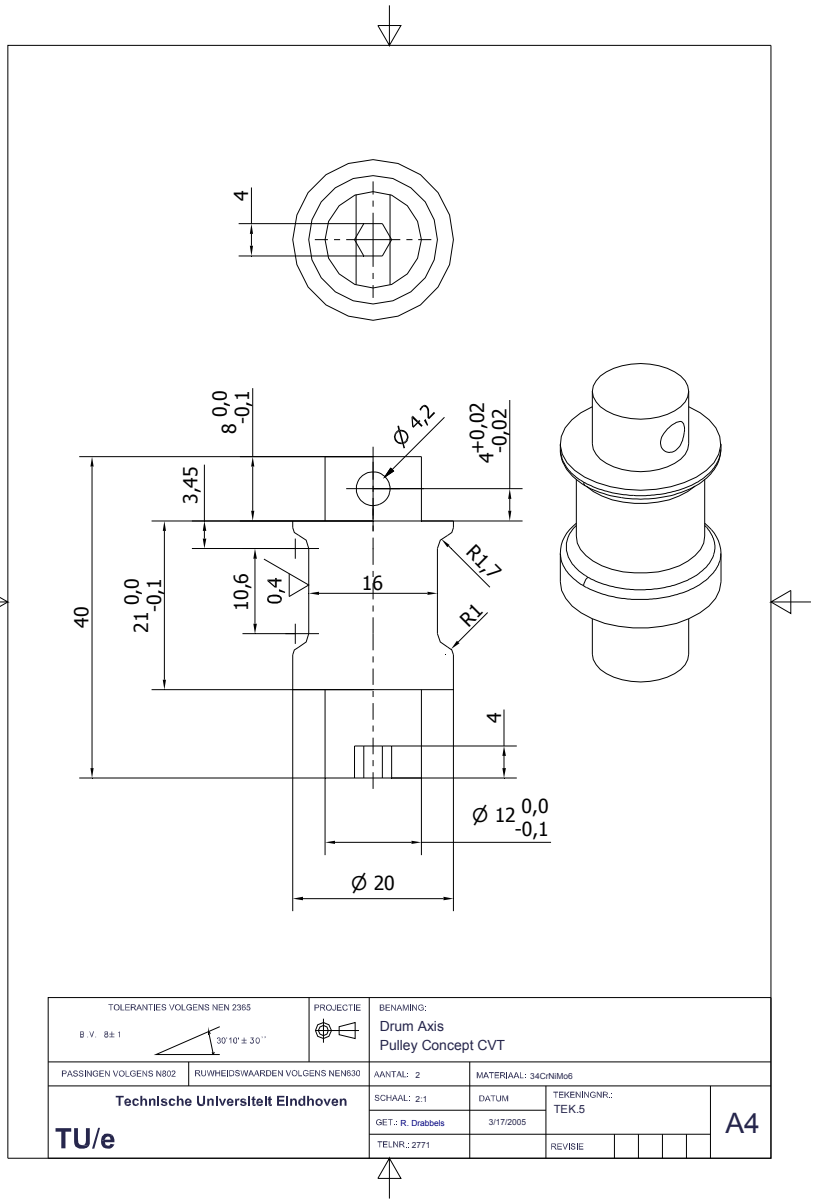

TOLERANTIES VOLGENS NEN 2365 B.V. 8± 1 30'10' ± 30''	PROJECTIE	BENAMING: Drum Axis Pulley Concept CVT	
PASSINGEN VOLGENS N802	RUWHEIDSWAARDEN VOLGENS NEN630	AANTAL: 2	MATERIAAL: 34CrNiMo6
Technische Universiteit Eindhoven TU/e		SCHAAL: 2:1 / GET.: R. Drabbels / TELNR.: 2771	DATUM: 3/17/2005 / REVISIE
		TEKENINGNR.: TEK.5	A4

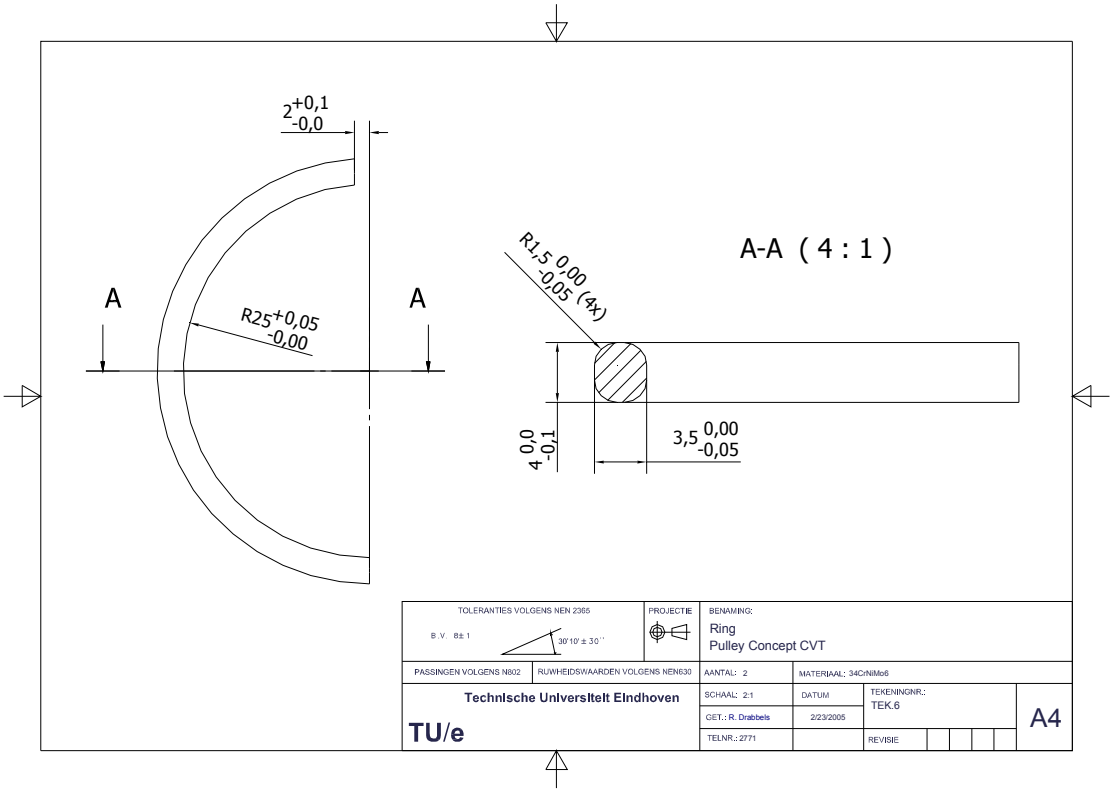
2 +0,1 -0,0
A
A
R25 +0,05 -0,00
A-A (4 : 1)
R1,5 0,00 -0,05 (4x)
4 0,0 -0,1
3,5 0,00 -0,05
TOLERANTIES VOLGENS NEN 2365
B.V. 8± 1
30'10' ± 3.0''
PROJECTIE
BENAMING:
Ring
Pulley Concept CVT
PASSINGEN VOLGENS N802
RUWHEIDSWAARDEN VOLGENS NEN630
AANTAL: 2
MATERIAAL: 34CrNiMo6
Technische Universiteit Eindhoven
TU/e
SCHAAL: 2:1
DATUM
TEKENINGNR.:
TEK.6
GET.: R. Drabbels
2/23/2005
A4
TELNR.: 2771
REVISIE

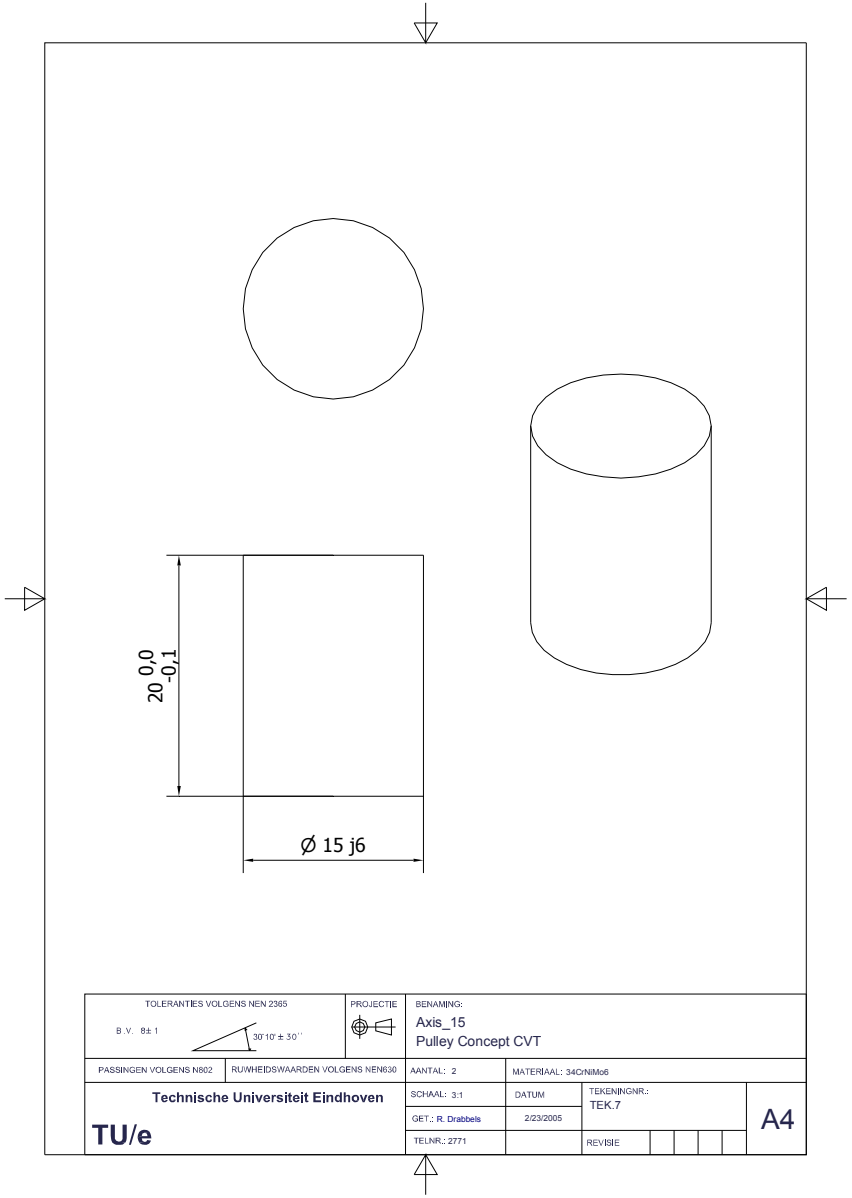

TOLERANTIES VOLGENS NEN 2365	PROJECTIE	BENAMING: Axis_15 Pulley Concept CVT	
B.V. 8± 1 30'10' ± 30''			
PASSINGEN VOLGENS N802	RUWHEIDSWAARDEN VOLGENS NEN630	AANTAL: 2	MATERIAAL: 34CrNiMo6
Technische Universiteit Eindhoven		SCHAAL: 3:1	DATUM: 2/23/2005
TU/e		GET.: R. Drabbels	TEKENINGNR.: TEK.7
		TELNR.: 2771	REVISIE
			A4

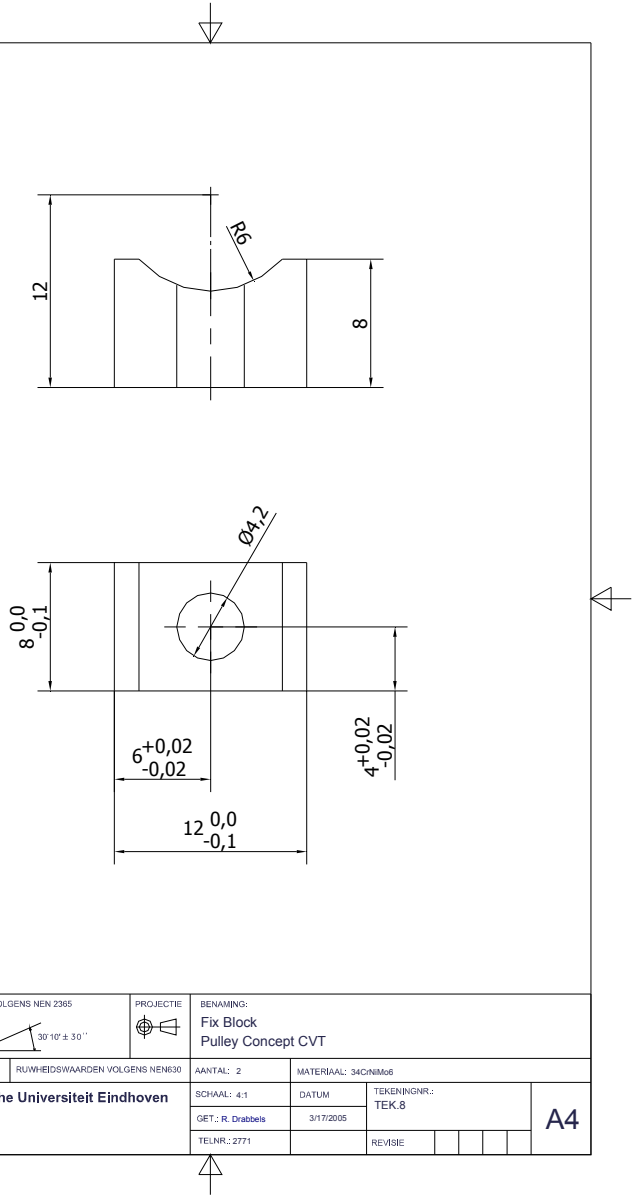

TOLERANTIES VOLGENS NEN 2365	PROJECTIE	BENAMING: Fix Block Pulley Concept CVT	
B.V. 8± 1 30'10' ± 30''			
PASSINGEN VOLGENS N802	RUWHEIDSWAARDEN VOLGENS NEN630	AANTAL: 2	MATERIAAL: 34CrNiMo6
Technische Universiteit Eindhoven		SCHAAL: 4:1	DATUM: 3/17/2005
TU/e		GET.: R. Drabbels	TEKENINGNR.: TEK.8
		TELNR.: 2771	REVISIE
			A4

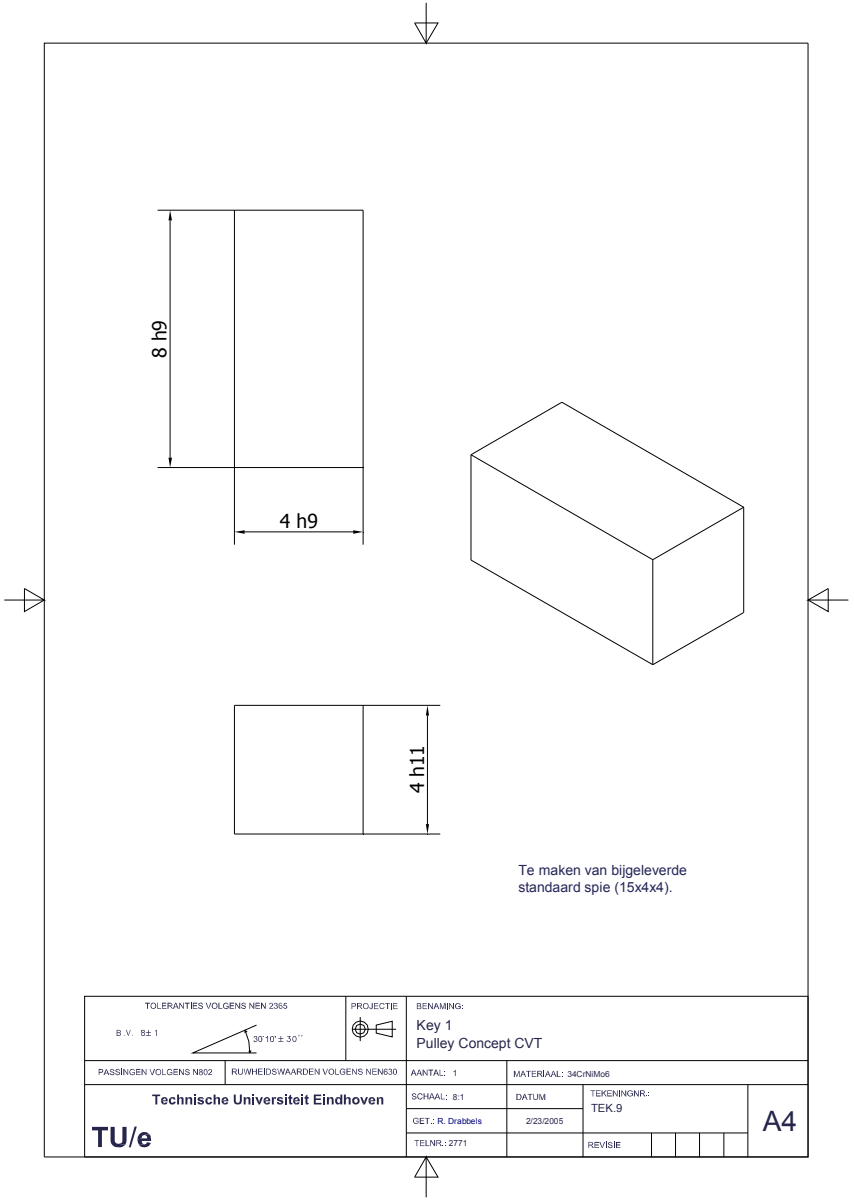

Te maken van bijgeleverde
standaard spie (15x4x4).

TOLERANTIES VOLGENS NEN 2365 B.V. 8± 1 30'10' ± 30''	PROJECTIE	BENAMING: Key 1 Pulley Concept CVT	
PASSINGEN VOLGENS N802	RUWHEIDSWAARDEN VOLGENS NEN630	AANTAL: 1	MATERIAAL: 34CrNiMo6
Technische Universiteit Eindhoven TU/e		SCHAAL: 8:1 GET.: R. Drabbels TELNR.: 2771	DATUM 2/23/2005 REVISIE
		TEKENINGNR.: TEK.9	A4

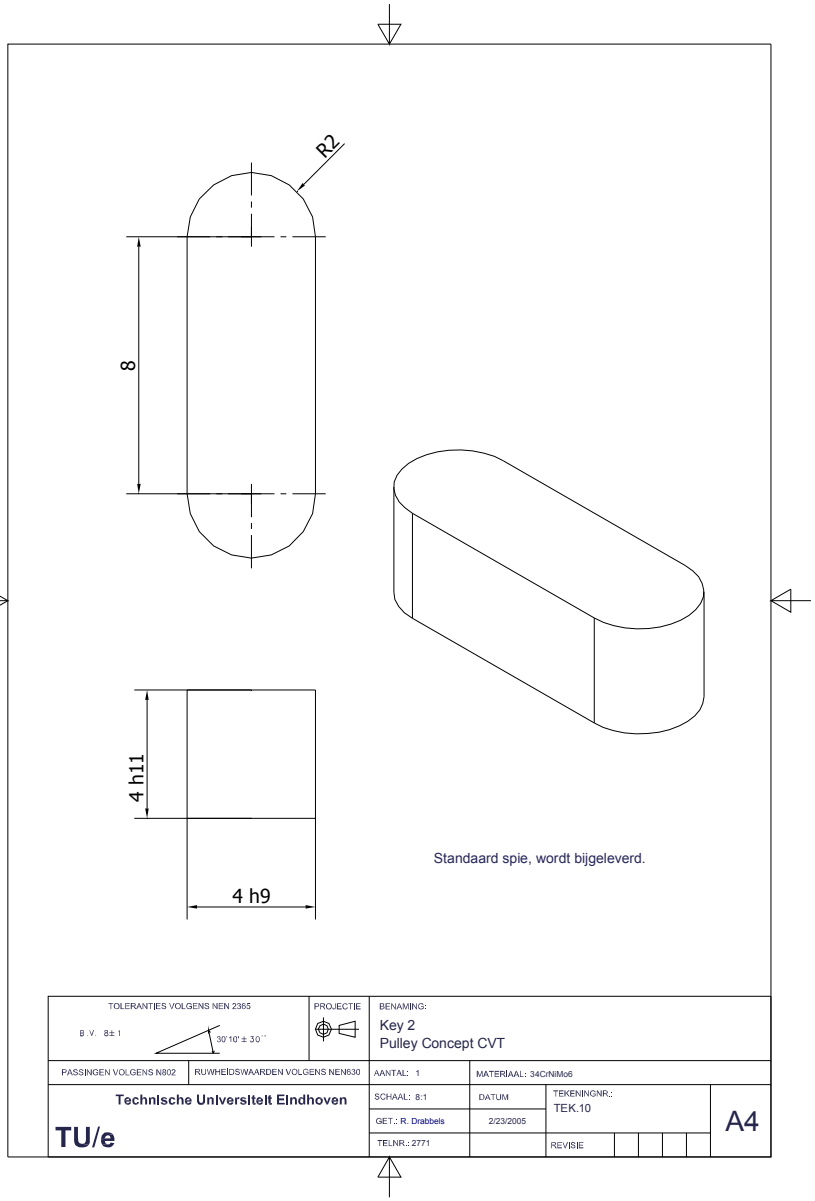

Standaard spie, wordt bijgeleverd.

TOLERANTIES VOLGENS NEN 2365 B.V. 8± 1 30'10' ± 30''	PROJECTIE	BENAMING: Key 2 Pulley Concept CVT	
PASSINGEN VOLGENS N802	RUWHEIDSWAARDEN VOLGENS NEN630	AANTAL: 1	MATERIAAL: 34CrNiMo6
Technische Universiteit Eindhoven TU/e		SCHAAL: 8:1 GET.: R. Drabbels TELNR.: 2771	DATUM 2/23/2005 REVISIE
		TEKENINGNR.: TEK.10	A4

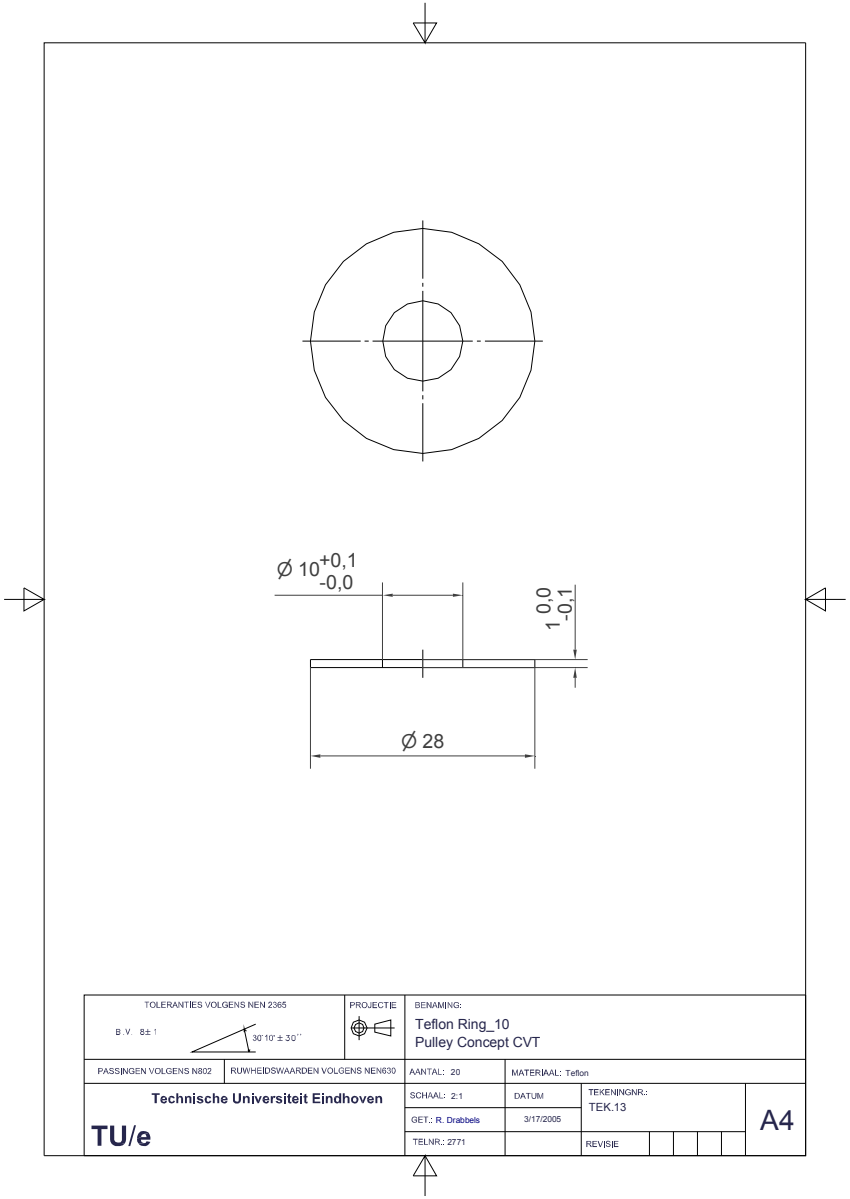

TOLERANTIES VOLGENS NEN 2365	PROJECTIE	BENAMING: Teflon Ring_10 Pulley Concept CVT	
B.V. 8± 1 30'10' ± 30''			
PASSINGEN VOLGENS N802	RUWHEIDSWAARDEN VOLGENS NEN630	AANTAL: 20	MATERIAAL: Teflon
Technische Universiteit Eindhoven		SCHAAL: 2:1	DATUM
		GET.: R. Drabbels	3/17/2005
TU/e		TELNR.: 2771	TEKENINGNR.: TEK.13
			REVISIE
			A4

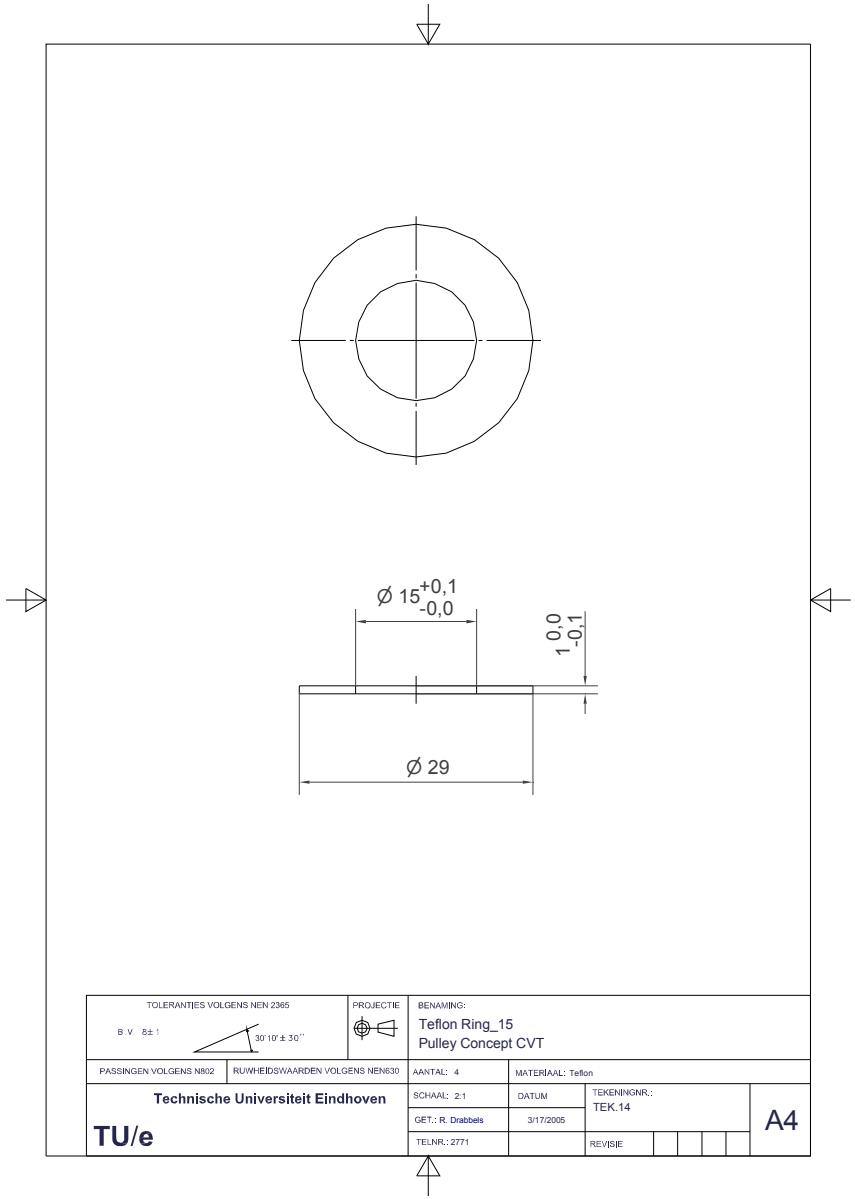

TOLERANTIES VOLGENS NEN 2365	PROJECTIE	BENAMING: Teflon Ring_15 Pulley Concept CVT	
B.V. 8± 1 30'10' ± 30''			
PASSINGEN VOLGENS N802	RUWHEIDSWAARDEN VOLGENS NEN630	AANTAL: 4	MATERIAAL: Teflon
Technische Universiteit Eindhoven		SCHAAL: 2:1	DATUM
		GET.: R. Drabbels	3/17/2005
TU/e		TELNR.: 2771	TEKENINGNR.: TEK.14
			REVISIE
			A4

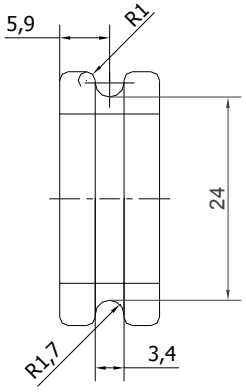

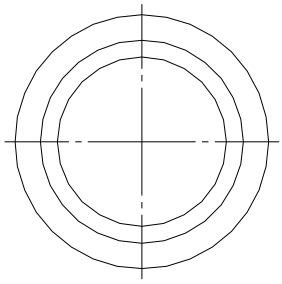

De lager-ringen worden bijgeleverd.

TOLERANTIES VOLGENS NEN 2365 B.V. 8± 1 ; 30'10" ± 30"	PROJECTIE	BENAMING: Bearing_10 Ring Pulley Concept CVT	
PASSINGEN VOLGENS N802	RUWHEIDSWAARDEN VOLGENS NEN630	AANTAL: 10	MATERIAAL:
Technische Universiteit Eindhoven TU/e		SCHAAL: 2:1 GET.: R. Drabbels TELNR.: 2771	DATUM: 2/23/2005 REVISIE
		TEKENINGNR.: TEK.11	A4

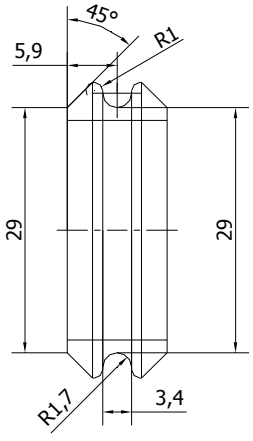

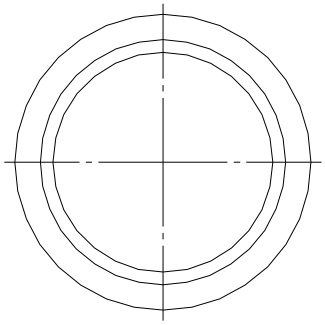

De lager-ringen worden bijgeleverd.

TOLERANTIES VOLGENS NEN 2365 B.V. 8± 1 ; 30'10" ± 30"	PROJECTIE	BENAMING: Bearing_15 Ring Pulley Concept CVT	
PASSINGEN VOLGENS N802	RUWHEIDSWAARDEN VOLGENS NEN630	AANTAL: 2	MATERIAAL:
Technische Universiteit Eindhoven TU/e		SCHAAL: 2:1 GET.: R. Drabbels TELNR.: 2771	DATUM: 2/23/2005 REVISIE
		TEKENINGNR.: TEK.12	A4

NOMENCLATURE AND ACRONYMS

Acronyms

Symbol	*Description*
ATF	Automatic Transmission Fluid
CAD	Computer Aided Design
CVT	Continuously Variable Transmission
DNR	Drive Neutral Reverse
EMPAct	Electromechanical Pulley Actuation system
FEM	Finite Element Method

Nomenclature

Symbol	*Description*	*Value [Unit]*
C	Bearing basic dynamic load rating	[N]
C_0	Bearing basic static load rating	[N]
D	Outer bearing diameter	[mm]
F	(Actuation) force	[N]
F_a	Axial bearing load	[N]
F_{clamp}	Clamping force	[N]
$F_{clamp,0}$	Friction loss constant	[N]
$F_{clamp,th}$	Theoretical clamping force (no loss)	[N]
F_N	Normal force	[N]
F_s	Pulley shaft shear force	[N]
F_w	Friction force between moveable ring and pulley shaft	[N]
L	Bearing basic rating life	[10^6 revolutions]
M_0	Bearing friction torque dependent on speed	[Nmm]
M_1	Bearing friction torque dependent on load	[Nmm]
P	Bearing load	[N]
P_0	Initial rope power	[W]
P_{in}	Roller system input power	[W]
P_{loss}	Power loss	[W]
P_{out}	Roller system output power	[W]
R	Rope running radius	[mm]
R_t	Roller tread radius	[mm]
T	Rope layer tensile force	[N]
T_0	Initial rope layer tensile force	[N]
T_{act}	Actuation torque	[Nm]
T_{shaft}	Pulley shaft torque	[Nm]
W	Frictional force between rope layers	[N]
c	Friction loss constant	[-]
d	Inner bearing diameter	[mm]
d_M	Mean bearing diameter	[mm]
f	Roller system output force	[N]
f_0	Bearing factor for frictional torque dependent on speed	[-]
f_1	Bearing factor for frictional torque dependent on load	[-]
i	Transmission ratio (output force / input force)	[-]
n	Bearing rotational speed	[rpm]
n_r	Number of rollers	[-]
p	Bearing life exponent	[-]
r	Rope radius	[mm]
v_0	Initial rope speed	[m/s]
v_{rel}	Relative speed between rope layers	[m/s]
v_{ring}	Moveable ring speed	[m/s]
α	Pulley wedge angle	11 [°]
η	Roller system efficiency	[-]
η_{est}	Estimated roller system efficiency	[-]
η_r	Rope efficiency	[-]
μ	Coefficient of friction between rope layers (Technora)	0.15 [-]
μ_R	Coefficient of friction between moveable ring and pulley shaft	0.1 [-]
ν	Bearing lubricant kinematical viscosity	0.12 [mm^2/s]
φ	Rope wrap angle	[rad]
ω_{drum}	Drum angular speed	[rad/s]

SAMENVATTING

Om het brandstofverbruik, de prestaties en het comfort van hedendaagse auto's te verbeteren wordt onderzoek gedaan naar continu variabele transmissies, ofwel CVTs. De meeste CVTs die verkocht worden, worden geactueerd met een hydraulisch systeem. Hydraulische actuatie lijdt echter onder grote verliezen in de oliepomp, welke de voornaamste oorzaak zijn van het relatief lage rendement van de meeste CVTs ten opzichte van handmatige transmissies. Om dit grote hydraulische vermogensverlies kwijt te raken en daarmee het rendement van de CVT te verbeteren, zijn verscheidene elektromechanische actuatieconcepten onderzocht. Vervolgens wordt een nieuw actuatieconcept voorgesteld met een overbrengverhouding op de poelie as, gecreeerd met behulp van een katrolsysteem en een kabel. In het nieuwe actuatiesysteem is de actuatiekracht verlaagd, waardoor het vermogensverlies van het taatslager dat de actuatiekracht doorleidt naar de poelie as kleiner is. Er is een model gemaakt van het nieuwe actuatiesysteem en er zijn rendementsmetingen gedaan. Verder worden enkele voorstellen gedaan voor het complete transmissie ontwerp en de actuatie van de kabel.

Dit verslag omvat een paper dat geschreven is voor het *ASME Journal of Mechanical Design* en enkele bijlagen die een dieper inzicht geven in het ontwerpproces.

ACKNOWLEDGMENT

I would like to thank my coaches Koen van de Meerakker and Bram Bonsen for their support and guidance during the project, and for their help during the writing of my paper.
Furthermore I would like to thank Jan de Vries, Toon van Gils, Ruud van den Bogaert and Wietse Loor for helping me with the test setup.
Finally I would like to thank Janneke Zeebregts at the GTD for her help with the construction drawings, and all students in the AES laboratory for their support.